1-1-2018

Fracture Criterion for Surface Cracks in Plates under Remote Tension Loading

Taoufik El Mountassir

Fracture criterion for surface cracks in plates under remote tension loading

By

Taoufik El Mountassir

A Thesis
Submitted to the Faculty of
Mississippi State University
in Partial Fulfillment of the Requirements
for the Degree of Master of Science
in Aerospace Engineering
in the Department of Aerospace Engineering

Mississippi State, Mississippi

May 2018

Fracture criterion for surface cracks in plates under remote tension loading

By

Taoufik El Mountassir

Approved:

James C. Newman, Jr
(Major Professor)

Thomas E. Lacy
(Committee Member)

Rani Warsi Sullivan
(Committee Member)

Ratneshwar (Ratan) Jha
(Graduate Coordinator)

Jason M.Keith
Dean
Bagley College of Engineering

Name: Taoufik El Mountassir

Date of Degree: May 4, 2018

Institution: Mississippi State University

Major Field: Aerospace Engineering

Major Professor: James C. Newman, Jr

Title of Study: Fracture criterion for surface cracks in plates under remote tension loading

Pages in Study 65

Candidate for Degree of Master of Science

Surface-crack configurations are among the most important crack problems in the aerospace industry. The residual strength of a surface-cracked component is complicated by three-dimensional variation of the stress-intensity factor around the crack front and plastic deformations, which vary from plane stress at the free boundary, to nearly plane-strain behavior in the interior. In 1973, a two-parameter fracture criterion (TPFC) was developed to analyze fracture behavior of surface-crack configurations. Estimates were made around the crack front for fracture initiation—the critical parametric angle. Recently, NASA developed the Tool for Analysis of Surface Cracks (TASC) software that predicts critical location. This thesis is the application of the TPFC with the TASC critical angles using an equation developed from the TASC software. The TPFC was applied to three materials: a brittle titanium alloy, a ductile titanium alloy, and a ductile 301 stainless steel. The TPFC with the TASC critical angles correlated fracture behaviors well.

DEDICATION

I am dedicating my Master of Science thesis to each and every person who helped me achieve my goal, and who believed in me, my family, my professors and my friends.

A special feeling of gratitude goes to my loving parents, my mother Nezha, and my father Rachid. I hope I've made you two proud parents and I will eternally hope to be a good role model for my little brother Mahdi.

Although they are no longer of this world, their memories continue to regulate my life, to my paternal and maternal grandfathers, their love for me knew no bounds. I also take pleasure in dedicating this thesis to everyone in my close family, grandmothers, uncles, aunts and cousins. Each one of them has encouraged me to realize my dream and to keep pursuing it.

My Master of Science thesis is dedicated to all of the UIR staff who has helped me through the four years of college. My thesis would not be accomplished without the advice, the encouragement and the support of my major professor, Dr. Newman, to whom I dedicate this work.

ACKNOWLEDGEMENTS

First, I want to thank God, for all his blessings and for the power he always gives me to continue working even harder.

There have been many people who have walked along side me during the past five years, and I want to thank them from the bottom of my heart. Mum and Dad, thank you for guiding me, for placing opportunities in front of me, and for always leading me to the right path. But most of all, thank you for loving me unconditionally. Your presence has made me who I am today, if I aim to be excellent, it's only because you believed in me and my capacities, and I will forever be grateful.

I am also very grateful to Dr. James C. Newman, Jr., for the patient guidance, encouragement and advice he has provided throughout my time as his student. I have been extremely lucky to have a supervisor who cared so much about my work, and who responded to my questions and queries so promptly, from the early beginning of my research until the completion of this thesis. Furthermore, I would like to thank Dr. Thomas Lacy and Dr. Rani Warsi Sullivan for serving as members on my thesis committee.

Thank you, Mississippi State University, for the one life time experience.

TABLE OF CONTENTS

LIST OF TABLES

LIST OF FIGURES

NOMENCLATURE

A_g	Gross section area, mm^2
A_n	Net-section area, mm^2
a	Crack depth, mm
a_i	Initial crack depth, mm
c	Crack half-length, mm
c_i	Initial crack half-length, mm
E	Young's modulus of elasticity, MPa
F_n	Boundary-correction factor based on net-section stress
F_{NR}	Newman-Raju elastic boundary-correction factor
f_w	Width-correction factor
f_ϕ	Angular function derived from embedded elliptical crack solution
K	Stress-intensity factor, MPa-$m^{1/2}$
K_F	Elastic-plastic fracture toughness, MPa-$m^{1/2}$
K_{Ie}	Elastic stress-intensity factor at failure, MPa-$m^{1/2}$
K_ε	Plastic-strain-concentration factor
K_σ	Plastic-stress-concentration factor
m	Fracture ductility parameter

M_e	Elastic magnification factor on stress-intensity factor
P_F	Maximum applied load at failure, MPa
Q	Elastic shape factor for an elliptical crack
S	Applied stress, MPa
S_g	Gross section fracture stress, MPa
S_n	Net-section stress at fracture, MPa
t	Specimen thickness, mm
w	Specimen one-half width, mm
ε	Strain
ρ	Notch radius, mm
σ	Stress, MPa
σ_u	Ultimate tensile strength, MPa
σ_{ys}	Yield stress (0.2 percent offset), MPa
Φ	Complete elliptic integral of second kind
ϕ	Parametric angle, degree
ϕ_c	Critical parametric angle, degree
LEFM	Linear Elastic Fracture Mechanics
TASC	Tool for Analysis of Surface Cracks

CHAPTER I

INTRODUCTION

1.1 Overview

Surface cracks are the most predominant crack configuration in the aerospace industry. They usually nucleate and start to propagate from small imperfections or holes in structural components. A large number of researchers and scientists have tried to develop a solution for the stress-intensity factor for a semi-elliptical surface crack in a finite-thickness plate to obtain predictions of both fracture strength and fatigue-crack propagation.

The stress intensity factor, denoted as K, is used to predict the stress state around the surface-crack front subjected to remote loading. An exact solution for the stress-intensity factors around an elliptical crack in an infinite body subjected to remote uniaxial tension was given by Irwin [1] based on the analysis of Green and Sneddon [2]. However, there isn't an exact solution for the stress-intensity factors for a semi-elliptical surface crack in a finite-thickness plate, but a number of approximate numerical solutions and equations have been developed.

Irwin [1] developed an estimation of the stress-intensity factor for a semi-elliptical surface crack in finite-thickness plate, but it was only valid for a crack-depth-to-specimen-thickness ratio less than one-half thickness. Advanced calculations and approximations were conducted by others, such as Smith and Alavi [3], Kobayashi and Moss [4], Rice and Levi [5] and Smith [6].

In 1973, Newman [7] developed an equation for the stress-intensity factor for a semi-elliptical surface crack in a finite-thickness (t) plate as a function of both crack-depth-to-thickness (a/t) and crack-depth-to-crack-length (a/c) at an assumed critical fracture location for the parametric angle (ϕ_c). In 1979, Newman and Raju [8] developed an equation that gave a better approximation of the stress-intensity factor for both tension and bending loads with respect to the parametric angle ϕ, a/t and a/c using three-dimensional (3D) elastic finite-element analyses [9].

Linear-elastic fracture mechanics (LEFM) can only be applied to low fracture toughness materials, however for high toughness materials, the LEFM concept is no longer valid, and other methods must be considered. Since 1970, several researchers have tried to develop fracture criteria [10-13] for surface cracks in high toughness materials using elastic-plastic notch-strength analyses or fracture mechanics concepts. In 1973, a Two-Parameter-Fracture-Criterion (TPFC) was developed by Newman [7] using notch-strength analyses, similar to Kuhn [10]. The main advantage of this engineering approach is its simplicity. The TPFC equation is a function of K_{Ie}, net-section stress (S_n) at failure, material tensile properties, and two material fracture parameters, K_F and m. The elastic-plastic fracture toughness is K_F and m is a fracture ductility parameter.

The National Aeronautical and Space Administration (NASA) Marshall Space Flight Center (MSFC) has developed the Tool for Analysis of Surface Cracks (TASC) software. TASC uses MATLAB software and was developed by Allen and Wells [14, 15]. The software is used to predict the critical angles (ϕ_c) along a semi-elliptical surface-crack front where fracture nucleates for a wide range in crack-depth-to-thickness (a/t) ratios and crack-depth-to-crack-length (a/c) ratios less than or equal to one. TASC uses a methodoloy that was developed by Allen and Wells [14, 15] for the prediction of the critical parametric angle. The critical location along the surface-crack front is where the product of the T-stress and the J-integral maximises, similar to what Reuter et al. [11] and Leach et al. [12] had developed to predict the critical angle. The elastic T-stress (or the second term in the Williams series expansion) is the stress acting parallel to the crack plane and perpendicular to the crack front. The J-integral is the strain energy release rate for an elastic material and strength of the stress/strain state for a nonlinear elastic material. Herein, an equation for the critical angle as a function of a/t and a/c was developed based on the critical angles predicted from the TASC code.

In 1963, Smith [16] conducted fracture tests on surface cracks in rectangular sheets made of Ardeformed 301 stainless steel and two titanium alloys for application in missile motor cases. In the current research, these fracture test data were used to determine the elastic-plastic fracture toughness parameters, and to predict the elastic stress-intensity factor at failure (K_{Ie}) using the newly developed equation for the critical parametric angle (ϕ_c), where fracture is predicted to initiate along a surface-crack front. The critical angle equation is a function of surface-crack configuration (a/t and a/c) and was independent of the material's strain-hardening properties

Once the critical angles were found, they were then used to calculate K_{Ie} using the Newman-Raju [8] stress-intensity factor equation for a semi-elliptical surface crack under remote tension loads. A TPFC analysis was conducted on each material data set to determine the two fracture parameters (K_F and m). A comparison was then made between the experimental and calculated K_{Ie} values for Ti-6Al-6V-2Sn, Ti-6Al-4V and 301 stainless steel as a function of the net-section stress at failure or other crack-configuration parameters.

1.2 Crack configuration and loading

Different configuration parameters characterize the surface-crack specimen, as shown in Figure 1.1. The parameters that describe the semi-elliptical surface-crack specimen are thickness (t), height (2h), width (2w), crack depth (a) and crack length (2c). For convenience and simplification, some terms are described in geometrical ratios, relating the crack size to specimen dimensions, like a/c describes the crack-depth-to-crack-length ratio, a/t for the crack-depth-to-specimen-thickness ratio, c/w for crack-length-to-specimen-width ratio, and the parametric angle ϕ are used to develop equations for stress-intensity factor along the crack front or to present the fracture data as a function of these ratios. Specimen height (2h) is selected large enough to have essentially no influence on the stress-intensity factor.

Plane–stress conditions are defined to be a state of stress in which the normal stress directed perpendicular to the x-y plane (see Fig. 1.1) and shear stresses in the x-y plane are assumed to be zero, while the plane-strain conditions are defined to be a state of strain in which the normal strain to the x-y plane and the shear strains in the x-y plane are assumed to be zero. Along the surface-crack front, the state-of-stress changes from plane stress at the free surface to the nearly plane strain condition at the maximum depth location.

In this study, only the behaviour of surface cracks under remote tension loading was examined; further analyses are required for remote bending. The stress-intensity factor equations for remote bending [8, 9] have been developed, and fracture test data for remote bending [11, 12] has also been obtained for some materials. But further studies are required for the critical parametric angle under remote bending.

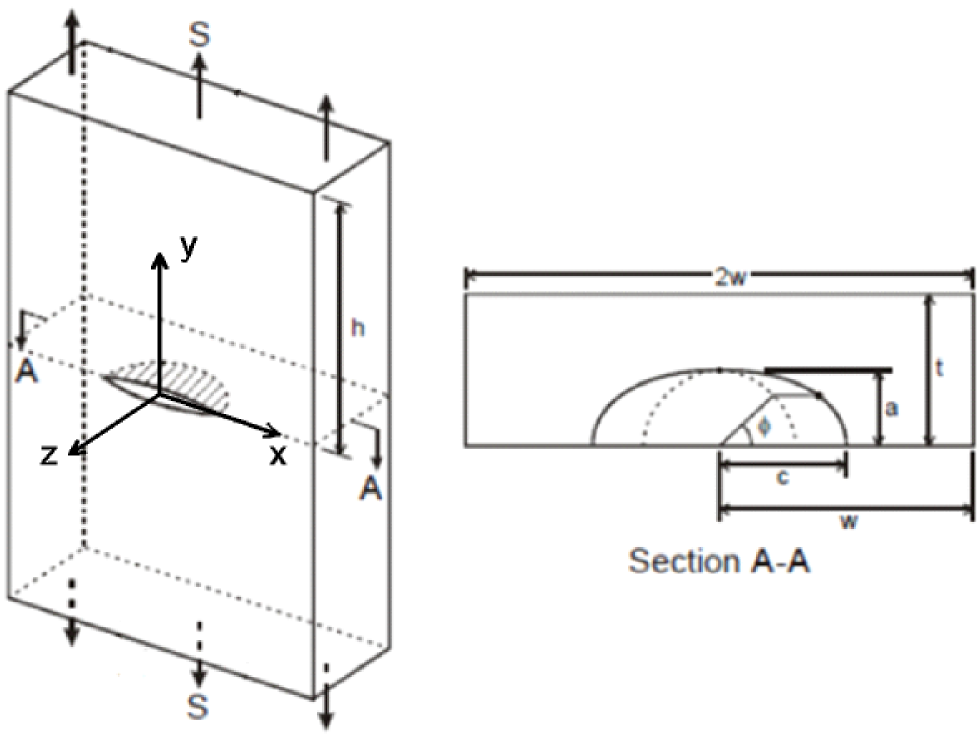

Figure 1.1 Surface-crack configuration.

CHAPTER II

MATERIAL AND SPECIMEN CONFIGURATION

Several alloys were tested with surface cracks in thin sheets by Smith [16]. They were Ti-6Al-6V-2Sn and Ti-6Al-4V titanium alloys, and Ardeformed 301 stainless steel, for potential application in solid-propellant rocket-motor cases. Fracture test data were generated for various crack depths and crack lengths in flat sheet specimens. These data were then used to determine the stress-intensity factor at failure (K_{Ie}) using the Newman-Raju equation [8] with the proposed equation for the critical parametric angle at fracture. The three materials and the specimen configurations are described herein.

2.1 Ti-6Al-6V-2Sn titanium alloy

Titanium alloys are widely used in the aerospace and automotive industries. They are characterized by several advantages, among them is the high-strength-to-weight ratio. Titanium alloys have demonstrated more reliability and to be more cost-efficient by replacing heavier and more costly materials. That is why they have been chosen for rocket motor cases and other applications.

The Ti-6Al-6V-2Sn titanium alloy is an alpha-beta alloy. It is characterized by superior strength and corrosion resistance making it very adaptable for several uses. The composition of the alloy is given in Table 2.1.

Table 2.1 Composition of Ti-6Al-6V-2Sn titanium alloy.

Material	Al	V	Sn	Cu	Fe	C	N_2	H_2	Ti
Ti-6Al-6V-2Sn	5.5	5.4	2	0.67	0.73	0.03	0.03	0.01	Bal.

The uniaxial tensile properties of the Ti-6Al-6V-2Sn alloy are shown in Table 2.2. The titanium alloy has very little directionality. The yield stress and tensile strength in the longitudinal direction is only about 44 MPa higher than the transverse direction.

Table 2.2 Room temperature tensile properties for Ti-6Al-6V-2Sn alloy.

Test Direction	Yield stress (0.2%), MPa	Ultimate strength, MPa
Longitudinal	1275	1348
Transverse	1233	1302

The fracture test data were obtained from Smith [16] for surface cracks under remote tension loadings for a wide range of crack-depth-to-crack-length (a_i/c_i) ratios from 0.4 to 0.77, crack-depth-to-specimen-thickness (a_i/t) ratios ranging from 0.2 to 0.63, and crack-length-to-specimen-width (c_i/w) ratios from 0.06 to 0.3. Tables 2.3 and 2.4 show the fracture test data for the Ti-6Al-6V-2Sn alloy for longitudinal and transverse directions, respectively.

Table 2.3 Fracture test data for Ti-6Al-6V-2Sn in longitudinal direction.

Test direction	Crack configuration (a)		Net area, mm^2	S_n/σ_u	Failure load, kN	Failure stress, MPa	
	a_i, mm	c_i, mm				Gross	Net
Long.	0.508	0.762	60.38	0.778	63.38	1040	1050
Long.	0.762	0.9906	59.48	0.621	49.82	820.4	838.2
Long.	0.8636	1.4605	58.96	0.576	45.81	752.9	777.6
Long.	1.143	1.7145	57.22	0.516	39.81	659.1	696.2
Long.	1.27	2.2225	56.71	0.462	35.36	578	624
Long.	1.27	2.8575	55.03	0.394	29.24	481.1	531.8
Long.	1.524	3.175	52.58	0.376	26.69	442.8	508
Long.	1.6002	3.6195	51.3	0.344	23.8	394.8	464

(a) Average thickness (t) is 2.54 mm, and average width (w) is 12.7 mm.

Table 2.4 Fracture test data for Ti-6Al-6V-2Sn in transverse direction.

Test direction	Crack configuration (a)		Net area, mm^2	S_n/σ_u	Failure load, kN	Failure stress, MPa	
	a_i, mm	c_i, mm				Gross	Net
Trans.	0.508	0.762	60.32	0.883	69.39	1140	1151
Trans.	0.508	0.8255	60.96	0.871	69.17	1123	1135
Trans.	1.016	1.4605	59.22	0.536	41.36	672.6	699
Trans.	1.0922	1.5875	58.58	0.56	42.7	697.2	729.5
Trans.	1.143	2.2225	58.19	0.438	33.25	535	571.8
Trans.	1.3462	2.2225	55.93	0.479	34.91	578	624.7
Trans.	1.27	2.8575	55.29	0.446	32.13	533.1	581.7
Trans.	1.524	2.7305	54.58	0.453	32.25	528.2	591.3
Trans.	1.524	3.7211	52.06	0.408	27.69	455	532.2
Trans.	1.524	3.8735	51.61	0.39	26.24	427.6	508.8

(a) Average thickness (t) is 2.54 mm, and average width (w) is 12.7 mm.

2.2 Ti-6Al-4V titanium alloy

The Ti-6Al-4V titanium alloy is the most widely used titanium alloy in aerospace applications, and that is due to its outstanding strength-to-weight ratio, resistance to very high temperatures, high formability, and corrosion resistance. Thus, it was considered for use in missile motor cases. Also, it is always considered as a baseline for comparison with other titanium alloys. Table 2.5 shows the composition of Ti-6Al-4V alloy; and Table 2.6 shows the uniaxial tensile properties for the alloy in both the longitudinal and transverse directions.

Table 2.5 Composition of Ti-6Al-4V titanium alloy.

Material	Al	V	Fe	C	N_2	H_2	Ti
Ti-6Al-4V	6	4.1	0.09	0.019	0.016	0.008	Bal.

Table 2.6 Room temperature tensile properties for Ti-6Al-4V titanium alloy.

Test Direction	Yield stress (0.2%), MPa	Ultimate strength, MPa
Longitudinal	1036	1132
Transverse	1038	1127

As with the Ti-6Al-6V-2Sn alloy, the Ti-6Al-4V alloy has very little directionality. Essentially, the yield stress and ultimate tensile strength are identical.

The fracture test data was obtained from Smith [16] for surface cracks under remote tension loading. Tables 2.7 and 2.8 give the test data for longitudinal and transverse directions, respectively. For these data, the a_i/c_i ratio ranged from 0.33 and 0.8 and a_i/t ranged from 0.05 to 0.58.

Table 2.7 Fracture test data for Ti-6Al-4V in longitudinal direction.

Test direction	Crack configuration (a)		Net area, mm^2	S_n/σ_u	Failure load, kN	Failure stress, MPa	
	a_i, mm	c_i, mm				Gross	Net
Long.	0.127	0.381	67.74	1.026	78.73	1161	1161
Long.	0.381	0.6985	66.45	1.034	77.85	1159	1170
Long.	0.508	0.889	67.74	1.003	76.95	1124	1135
Long.	0.889	1.397	65.8	1.016	75.73	1117	1150
Long.	1.143	1.905	64.516	0.983	71.83	1059	1112
Long.	1.143	1.905	65.16	0.97	71.61	1046	1098
Long.	1.27	2.4765	61.93	0.961	67.39	1003	1087
Long.	1.397	2.6035	61.93	0.945	66.27	977.7	1069
Long.	1.4732	3.302	60	0.907	61.6	908.8	1026
Long.	1.4478	3.4925	58.71	0.905	60.16	904.7	1024

(a) Average thickness (t) is 2.54 mm, and average width (w) is 13.35 mm.

Table 2.8 Fracture test data for Ti-6Al-4V in transverse direction.

Test direction	Crack configuration (a)		Net area, mm^2	S_n/σ_u	Failure load, kN	Failure stress, MPa	
	a_i, mm	c_i, mm				Gross	Net
Trans.	0.508	0.635	67.74	1.017	77.62	1134	1145
Trans.	0.5588	0.762	63.38	1.008	77.62	1124	1134
Trans.	0.8382	1.2065	67.1	1.006	76.06	1112	1133
Trans.	0.889	1.27	66.45	0.994	74.39	1087	1119
Trans.	0.8636	1.27	66.45	1.004	75.17	1099	1130
Trans.	1.0414	1.905	65.8	0.978	72.5	1050	1101
Trans.	1.143	1.8415	66.45	0.958	71.72	1029	1079
Trans.	1.1684	2.7178	63.87	0.912	65.61	949.7	1026
Trans.	1.3462	2.54	63.87	0.918	66.05	956.2	1034
Trans.	1.4478	3.302	60.64	0.892	60.94	890.5	1004
Trans.	1.4732	3.2385	61.93	0.927	64.72	928.8	1045

(a) Average thickness (t) is 2.54 mm, and average width (w) is 13.35 mm.

2.3 Ardeformed 301 stainless steel

The 301 stainless steel is characterized by its high fracture toughness, and the stainless properties of the material make it very promising to be used in various parts of missile motor cases. The steels that Smith [16] tested with surface cracks were at three different strength levels.

Table 2.9 gives the room-temperature tensile properties for the three 301 stainless steels. For convenience, the steels have been denoted as steels A, B and C.

Table 2.9 Room-temperature tensile properties for Ardeformed 301 stainless steel at various strength levels.

Material	Cryogenic tensile prestress, MPa	Heat treatment (aging cycle)	Yield stress (0.2%), MPa	Ultimate strength, MPa
Steel A	1724	20 hr at 800 F	2079	2082
Steel B	1551	20 hr at 800 F	1969	1991
Steel C	1724	None	1741	1745

The various strength levels were obtained by aging and processing the steels and the ultimate tensile strengths varied by 1745 to 2082 MPa. The fracture test data that Smith [16] generated used a wide range of crack-depth-to-length ratios from 0.27 to 0.63, and crack-depth-to-specimen-thickness ratios ranging from 0.42 to 0.88. Tables 2.10 to 2.12 give the fracture test data for the various strength levels of the 301-stainless steel.

Table 2.10 Fracture test data for Ardeformed 300 stainless-steel (A).

Steel A						
Crack configuration (a)		Net area, mm^2	S_n/σ_u	Failure Load, kN	Failure stress, MPa	
a_i, mm	c_i, mm				Gross	Net
0.7366	1.1684	67.67	1.046	147.5	2136	2179
0.7112	1.3208	73.35	1.008	154	2058	2100
0.8382	1.524	70.25	0.991	145	2007	2064
1.016	2.4003	70.32	0.953	139.6	1881	1985
1.1176	3.0988	67.48	0.905	127.2	1745	1885
1.0414	3.5052	69.09	0.839	120.8	1614	1748

(a) Average thickness (t) is 1.27 mm, and average width (w) is 28.82 mm.

Table 2.11 Fracture test data for Ardeformed 300 stainless-steel (B).

Steel B						
Crack configuration (a)		Net area, mm^2	S_n/σ_u	Failure Load, kN	Failure stress, MPa	
a_i, mm	c_i, mm				Gross	Net
0.9652	1.0287	71.93	1.051	150.6	2047	2093
0.8128	1.4859	72.9	1.017	147.7	1973	2026
0.9398	2.4511	71.87	0.937	134.1	1777	1866
1.0414	3.0861	69.8	0.94	130.7	1746	1872
1.0414	3.2385	70.19	0.915	127.9	1694	1822
1.1176	4.1021	68.32	0.906	123.2	1632	1803

(a) Average thickness (t) is 1.27 mm, and average width (w) is 28.82 mm.

Table 2.12 Fracture test data for Ardeformed 300 stainless-steel (C).

Steel C						
Crack configuration (a)		Net area, mm^2	S_n/σ_u	Failure Load, kN	Failure stress, MPa	
a_i, mm	c_i, mm				Gross	Net
0.5334	1.0287	71.99	0.984	123.7	1696	1718
0.7112	1.4732	71.87	0.981	123	1672	1711
1.016	2.1209	68.83	0.948	113.9	1576	1654
0.9652	2.3876	67.35	0.942	110.8	1561	1644
1.0414	2.7432	67.09	0.931	109	1522	1624
0.9906	3.2639	67.09	0.916	107.2	1484	1598

(a) Average thickness (t) is 1.27 mm, and average width (w) is 28.82 mm.

CHAPTER III

STRESS-INTENSITY-FACTOR EQUATIONS FOR SURFACE CRACKS.

3.1 Elastic stress-intensity factor

The concept of the stress-intensity factor, K, was developed by Irwin [17] in 1957. The stress-intensity factor is considered as one of the most important concepts in the field of Fracture Mechanics and it is used to describe the stress and strain state around the crack front in a linear-elastic material caused by loading on the cracked body.

Near the crack tip, the singularity $\frac{1}{\sqrt{r}}$ dominates the stress field. The stress-intensity factor is the strength of the singularity and can be used in different loading modes. These modes are defined as K_I (mode I) denoted as the opening mode (most dominant mode in applications), K_{II} (mode II) used for sliding mode (in-plane shear), and K_{III} (mode III) for tearing mode (out-of-plane shear). An equation relating the stress-intensity factor, the stress distribution near the crack tip and the singularity is shown as:

$$\sigma_{ij} = \left[\frac{K}{\sqrt{2\pi r}} f_{ij}(\theta)\right] + higher\ order\ terms \tag{3.1}$$

At fracture, the stress-intensity factor is at its critical value and can be denoted as K_{Ic}, the plane-strain fracture toughness, for low-toughness materials, such as glass or high-strength steels. However, in general, the critical K value at failure is not a constant, but varies with crack length, component size, and type of loading (tension or bending). Non-linear or elastic-plastic fracture mechanics concepts are required to correlate and to predict the failure of cracked components in structures made of more ductile materials.

In this research, the stress-intensity factor equations for a surface crack in a flat sheet are reviewed. These equations are needed to show how the critical K value at failure, denoted herein as K_{Ie}, varies with surface-crack shape (a/c) and size (a/t) for brittle and ductile materials. In particular, fracture analyses will be conducted on the three materials selected for this study (Ti-6Al-6V-2Sn, Ti-6Al-4V and 301 stainless steel).

3.2 Newman equation (1973)

An equation for the stress-intensity factor around an elliptical crack in an infinite elastic solid under remote tension loading was derived by Irwin [1] based on the work of Green and Sneddon [2]. The equation gives the stress-intensity factor around the elliptical crack front and is given by:

$$K_I(\phi) = \frac{S\sqrt{\pi a}}{\Phi}\left(\frac{a^2}{c^2}cos^2\phi + sin^2\phi\right)^{\frac{1}{4}} \tag{3.2}$$

where S is the uniaxial stress acting normal to the plane of the crack, and Φ is the complete elliptic integral of second kind and is given by:

$$\Phi = \int_0^{\frac{\pi}{2}}\left(sin^2\phi + \left(\frac{a}{c}\right)^2 cos^2\phi\right)^{\frac{1}{2}} d\phi \tag{3.3}$$

In 1973, Newman developed a stress-intensity factor equation based on the numerical results from several researchers [3, 5, 18] for a surface crack in a finite-thickness and finite-width plate. He had selected, by engineering judgment, the critical location along the surface-crack front where fracture would initiate. Thus, the K equation was independent of the parametric angle, ϕ. The elastic stress-intensity factor for a semielliptical crack in a finite plate subjected to a remote tensile loading was:

$$K_{Ie} = S_g\sqrt{\pi\frac{a}{Q}}\,M_e \tag{3.4}$$

where S_g is the remote gross stress, a is the crack depth, the shape factor $Q = \Phi^2$, and M_e is the elastic-magnification factor. M_e is calculated by:

$$M_e = \left[M_1\left(\sqrt{Q\frac{c}{a}} - M_1\right)\left(\frac{a}{t}\right)^p\right]\sqrt{sec\left[\frac{\pi c}{2w}\left(\frac{a}{t}\right)\right]} \tag{3.5}$$

$$p = 2 + 8\left(\frac{a}{c}\right)^3 \tag{3.6}$$

For values of $a/c \leq 1$:

$$Q = 1 + 1.47\left(\frac{a}{c}\right)^{1.64} \tag{3.7}$$

$$M_1 = 1.13 - 0.1\left(\frac{a}{c}\right) \quad for \;\; 0.02 \leq \frac{a}{c} \leq 1.0 \tag{3.8}$$

For values of $a/c > 1$:

$$Q = 1 + 1.47\left(\frac{c}{a}\right)^{1.64} \tag{3.9}$$

$$M_1 = \sqrt{\frac{c}{a}}\left(1 + 0.03\frac{c}{a}\right) \tag{3.10}$$

In the limit as a/c approaches zero (an edge crack, Q = 1), equation (3.5) is fairly close to the stress-intensity factor solution for the single-edge-crack configuration [18]. The single-edge-crack stress-intensity factor equation is

$$M_e = 1.12 - 0.23\left(\frac{a}{t}\right) + 10.55\left(\frac{a}{t}\right)^2 - 21.71\left(\frac{a}{t}\right)^3 + 30.38\left(\frac{a}{t}\right)^4 \tag{3.11}$$

3.3 Newman-Raju equation (1979)

Accurate stress-intensity factors are required to predict surface-crack propagation life and fracture strength successfully. Many investigators have used numerical analyses and experimental methods to determine the stress-intensity factor for surface cracks in finite plates. In 1979, Newman [19] reviewed the stress-intensity factor solutions in the literature and found major discrepancies among the many solutions. He made an assessment on the fracture of surface cracks in a brittle epoxy and found that the Newman and Raju [8, 9] equation gave the best correlation.

In 1986, Newman and Raju [20] developed equations for stress-intensity factors for a wide range of three-dimensional crack configurations that are either subjected to uniform remote tension or bending loads. The equations were functions of several configuration parameters, crack depth (a), crack length (c), plate thickness (t), plate width (w) and the parametric angle (ϕ). Newman and Raju [8] developed the K equations for remote tension and bending for values of a/c ≤ 1 by fitting to finite-element results [9]. In 1986, they developed an equation for values of a/c greater than unity [20].

The Newman-Raju stress-intensity factor, K, along the crack front for a semi-elliptical surface crack in a finite plate for both remote tension and bending loads is calculated using:

$$K = (S_t + H_s S_b)\left(\frac{\pi a}{Q}\right)^{\frac{1}{2}} F_{NR}\left(\frac{a}{c}, \frac{a}{t}, \frac{c}{w}, \phi\right) \tag{3.12}$$

where:

$$F_{NR} = \left[M_1 + M_2\left(\frac{a}{t}\right)^2 + M_3\left(\frac{a}{t}\right)^4\right] g f_\phi f_w \tag{3.13}$$

$$H_s = H_1 + (H_2 - H_1)\, sin^p \phi \tag{3.14}$$

In this paper, only the remote tension load is considered. Thus, the equation becomes

$$K = S_t\left(\frac{\pi a}{Q}\right)^{\frac{1}{2}} F_{NR} \tag{3.15}$$

where S_t is the gross tensile stress and can be replaced by S_g, Q is the elastic shape factor for an elliptical crack, and F_{NR} is the Newman-Raju boundary correction factor. The finite-width correction factor, f_w, is:

$$f_w = \left[\sec\left(\frac{\pi c}{2w}\sqrt{\frac{a}{t}}\right)\right]^{\frac{1}{2}} \tag{3.16}$$

The other functions in the equation are dependent on the value of crack shape (a/c) and size (a/t).

For values of a/c ≤ 1:

$$M_1 = 1.13 - 0.09\frac{a}{c} \tag{3.17}$$

$$M_2 = -0.54 + \frac{0.89}{0.2+\frac{a}{c}} \tag{3.18}$$

$$M_3 = 0.5 - \frac{1}{0.65+\frac{a}{c}} + 14\left(1-\frac{a}{c}\right)^{24} \tag{3.19}$$

$$\mathrm{g} = 1 + \left[0.1 + 0.35\left(\frac{\mathrm{a}}{\mathrm{t}}\right)^2\right](1-\sin\phi)^2 \tag{3.20}$$

$$\mathrm{Q} = 1 + 1.464\left(\frac{a}{c}\right)^{1.65} \tag{3.21}$$

$$f_\phi = \left[\left(\frac{a}{c}\right)^2 cos^2\phi + sin^2\phi\right]^{\frac{1}{4}} \tag{3.22}$$

For values of a/c > 1:

$$M_1 = \left(\frac{c}{a}\right)^{\frac{1}{2}}\left(1+\frac{0.04c}{a}\right) \tag{3.23}$$

$$M_2 = 0.2\left(\frac{c}{a}\right)^4 \tag{3.24}$$

$$M_3 = -0.11\left(\frac{c}{a}\right)^4 \tag{3.25}$$

$$\mathrm{g} = 1 + \left[0.1 + 0.35\left(\frac{\mathrm{c}}{\mathrm{a}}\right)\left(\frac{\mathrm{a}}{\mathrm{t}}\right)^2\right] - (1-\sin\phi)^2 \tag{3.26}$$

$$\mathrm{Q} = 1 + 1.464\left(\frac{c}{a}\right)^{1.65} \tag{3.27}$$

$$f_\phi = \left[\left(\frac{c}{a}\right)^2 sin^2\phi + cos^2\phi\right]^{\frac{1}{4}} \tag{3.28}$$

For simplicity, and to be in accordance with the TPFC, another equation for the stress-intensity factor was used by replacing the gross stress (S_g) by net-section stress (S_n). The equation is expressed in terms of a net-section boundary correction factor (F_n) and depends on the crack configuration in the specimen, gross area and net-section area, and the equation is described below:

$$K_I = S_n \sqrt{\pi c}\, F_n\left(A_n, A_g, F_{NR}, c, a, Q\right) \tag{3.29}$$

where

$$F_n = \frac{A_g}{A_n} \sqrt{\frac{a}{cQ}}\, F_{NR} \tag{3.30}$$

where A_g = 2wt and A_n = 2wt - $\pi a_i c_i/2$. Equation (3.30) gives exactly the same stress-intensity factor as equation (3.15) for the same crack configuration and loading.

CHAPTER IV

TWO-PARAMETER FRACTURE CRITERION

In 1973, Newman [7] derived the Two-Parameter Fracture Criterion (TPFC). The fracture criterion was based on Inglis' [21] and Neuber's [22] equations. An equation that represents the elastic stress concentration at an elliptical hole in an infinite plate subjected to remote uniform stress, S, was developed by Inglis [21]. The elliptical hole had a major axis of 2c, minor axis of 2b, with root radius ρ. The stress-concentration equation is:

$$K_T = 1 + 2\sqrt{\frac{c}{\rho}} \tag{4.1}$$

When ρ = c, a circular hole, the exact stress-concentration factor is 3, but when the root radius goes to zero (a crack), the stress-concentration factor goes to infinity and the stress field is given by Irwin's equation (3.1). The elastic notch-root stress is $\sigma_e = S\,K_T$.

Neuber [22] developed an equation for elastic-plastic conditions at a notch root, a relation between the plastic-stress-concentration factor, K_σ, plastic-strain-concentration factor, K_ϵ, and the elastic stress-concentration factor, K_T.

$$K_\sigma K_\epsilon = {K_T}^2 \tag{4.2}$$

or

$$\sigma\,\epsilon\,E = {\sigma_e}^2 \tag{4.3}$$

where σ and ϵ are the local notch-root plastic stress and plastic strain, respectively, and ${\sigma_e}^2$ is the elastic notch-root stress.

Substituting equation (4.1) into equation (4.3) and setting S to S_n (net-section stress at failure), the plastic stress and plastic strain to their critical fracture values (σ_f, ε_f) and $\rho = \rho^*$ (assumed to be a constant at fracture) gives

$$K_F = \frac{K_{Ie}}{1-m\left(\frac{S_n}{\sigma_u}\right)} \; for \; S_n \leq \sigma_{ys} \tag{4.4}$$

$$\frac{K_{Ie}}{K_F} = 1 - m\left(\frac{S_n}{\sigma_u}\right) for \; S_n \leq \sigma_{ys} \tag{4.5}$$

The two fracture parameters (K_F, m) are functions of σ_f, ε_f, ρ^* and E, which are all assumed to be constant at fracture. The distance ρ^* is the distance ahead of the crack tip where the material separates due to void growth. S_n was normalized by ultimate tensile strength, σ_u, and K_{Ie} is the elastic stress-intensity factor at failure (see Ref. 7 for details on the derivation of the TPFC).

For the case where the nominal failure stress S_n is greater than the yield stress σ_{ys}, an approximate equation was also developed by Newman [23] as

$$\frac{K_{Ie}}{K_F} = \left(\frac{\sigma_{ys}}{S_n}\right)\left[1 - m\left(\frac{S_n}{\sigma_u}\right)\right] for \; S_n \geq \sigma_{ys} \tag{4.6}$$

The sensitivity of the material to the presence of the crack is described by the two fracture parameters K_F and m. The equation represents the characteristics of high-toughness materials if m = 1, and low-toughness materials when m is equal to zero. For the latter case, equation (4.4) is equivalent to LEFM at failure [7, 24].

The elastic stress-intensity factor at failue for a surface crack in a finite plate is a function of the net-section stress, initial crack length, c_i, the elastic net-section boundary correction factor, F_n, and is given by

$$K_{Ie} = S_n \sqrt{\pi c_i}\, F_n \tag{4.7}$$

To verify that the TPFC equation is a useful fracture criterion, Newman [7] conducted fracture analyses on many aluminum alloys, titanium alloys and steels for both surface and through cracks in sheets and plates. The TPFC was able to correlate the failure stresses within ±10% of the experimental failure stresses at both room and cryogenic temperatures.

In this research, fracture tests on surface-crack specimens made of two titanium alloys and steel [16] from the literature was analyzed using the TPFC [7], the Newman-Raju stress-intensity factor (K) equation [8], and the proposed equation for the critical fracture angle (ϕ_c) to see how well the new approach can correlate the fracture data.

CHAPTER V

ANALYSIS OF SURFACE CRACKS USING NASA TASC SOFTWARE

5.1 Critical parametric angle

The critical parametric angle is the location that is associated with fracture. Newman et al. [24] developed an equation to predict the surface-crack critical parametric angle, a multiplicative factor was used between two parameters, the stress-intensity factor $K(\phi)$ from the Newman-Raju equation [8] and the hyper-local normal-stress constraint factor $\alpha_h(\phi)$, the maximum of this multiplication is where the crack starts to fracture, ie. $(K\times \alpha_h)_{MAX}$. The maxima would have a high K value with a high value of constraint, which would be the most likely location for fracture initiation. The concept worked well on surface-cracked plates made of brittle D6ac steel under both remote tension and remote bending loads. The constraint factor was the average of the normal opening mode stresses in the plastic-zone region at a given parametric angle normalized by the ultimate tensile strength, and was calculated from 3D elastic-plastic finite-element analyses. On the other hand, Leach et al. [12] used the same constraint factor times the J-integral, $(J \times \alpha_h)_{MAX}$, where J is the J-integral [25] on the same material. Again, the concept worked very well on ductile D6ac steel with a wide range of surface-crack shapes and sizes.

The TASC (Tool for Analysis of Surface Cracks) software was developed by Allen and Wells [14, 15]. This software makes it easy to calculate the J-integral for surface-cracked plates under remote tension loads by interpolating between different surface-crack solutions. A large number of 3D elastic-plastic J-integral solutions for a wide range in surface-crack configurations in power-law hardening materials had been conducted and stored in the code. The software can interpolate results of crack shapes, $0.2 \leq a/c \leq 1$, and crack depths, $0.2 \leq a/t \leq 0.8$, from given surface-crack and plate cross-sectional dimensions and for the appropriate power-law hardening material property.

TASC software was mainly used to calculate the critical parametric angle for a semi-elliptical surface crack for different a/t and a/c ratios, and different strain-hardening coefficients, $3 \leq n \leq 20$, with $100 \leq E/\sigma_{ys} \leq 1000$ at different applied stress (S) levels. Figure 5.1 illustrates the stress-strain curve for different strain-hardening coefficients (n) for a given yield stress (σ_{ys} = 480 MPa) and elastic modulus (E = 72000 MPa). The stress-strain curve follows the linear plus power-law model (LPPL) as:

$$\frac{\varepsilon}{\varepsilon_{ys}} = \frac{\sigma}{\sigma_{ys}} \; for \; \varepsilon \leq \varepsilon_{ys} \tag{5.1}$$

$$\frac{\varepsilon}{\varepsilon_{ys}} = \left(\frac{\sigma}{\sigma_{ys}}\right)^{n} \; for \; \varepsilon > \varepsilon_{ys} \tag{5.2}$$

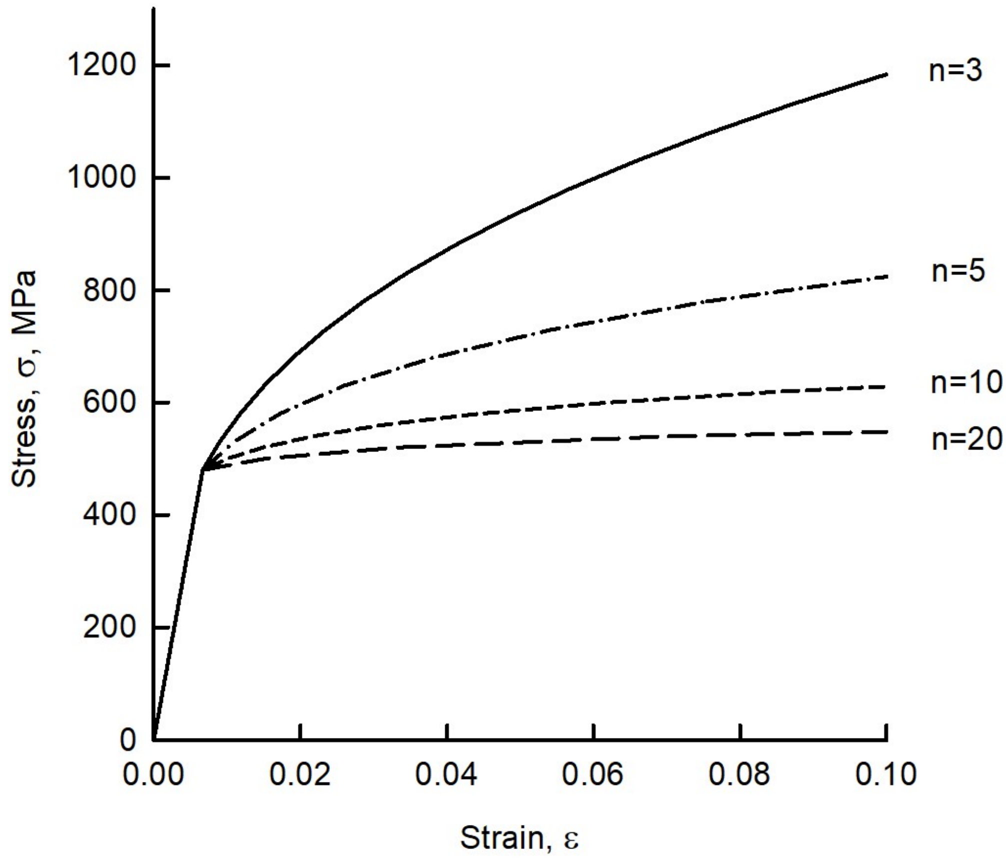

Figure 5.1 Stress-strain curve for different strain-hardening coefficient: n= 3, 5, 10 and 20.

The critical parametric angle, ϕ_c, is the location where the surface crack starts to grow, which is the location that is associated with fracture, but sometimes it is difficult to identify ϕ_c from inspection of the fracture surfaces. In this software, an estimation of ϕ_c is found based on equations developed by Allen and Wells [14, 15] for ASTM E2899 [13], which rely heavily on previous work done by others [11, 12, 24]. ϕ_c is found by finding the value of ϕ which maximizes the function, $f(\phi)$. The $f(\phi)$ equation is a function of $\frac{T(\phi)}{\sigma_{ys}}$ and $\frac{J(\phi)}{J_p}$ and is described as:

$$f(\phi) = \frac{J(\phi)}{J_p}\left(\frac{T(\phi)}{\sigma_{ys}} + 1\right) for\ \frac{T(\phi)}{\sigma_{ys}} \leq 0 \tag{5.3a}$$

$$f(\phi) = \frac{J(\phi)}{J_p}\left(\frac{T(\phi)}{4\sigma_{ys}} + 1\right) for\ \frac{T(\phi)}{\sigma_{ys}} > 0 \tag{5.3b}$$

Given that $\frac{T(\phi)}{\sigma_{ys}}$ is a linear-elastic concept and was found using the normalized T-stress tables [14] for surface cracks in tension for different crack configurations a/t and a/c and different parametric angle ϕ. Allen and Wells used the finite-element evaluations of Wang [26] and Wang and Bell [27]. The equation for $J(\phi)$ was normalized by J_p in order for $f(\phi)$ to be dimensionless without affecting the value for the critical angle. For convenience, a high-stress level ($S/\sigma_{ys} \sim 1$) was used to find the critical parametric angle values from the TASC software for application to surface cracks in ductile materials. Figure 5.2 shows an example on how the critical fracture angle was found following eq. 5.3.

Along the surface-crack front, the elastic T-stress and the stress-intensity factor K vary with crack size, a/t, and shape, a/c. For a semi-circular surface crack, a/c = 1, the stress-intensity factor is maximum at the free surface (ϕ = 0˚) and minimum at the maximum depth location (ϕ = 90˚). On the other hand, the normalized T-stress is at a minimum near the free surface (ϕ = 5˚) and starts to increase toward the maximum depth location for small crack sizes (a/t). By increasing a/t, the normalized T-stress starts to decrease toward the maximum depth location (ϕ = 90˚). For a/c = 1 and low applied-stress, the J-integral is at a maximum value at the free surface and starts to decrease toward the maximum depth location. However, for high-applied stress level the J-integral starts increasing from ($\phi = 0^{\circ}$), reaches a maximum value at of about 24˚, and decreases towards the maximum depth location ($\phi = 90^{\circ}$).

In other hand, for $0.2 \leq a/c \leq 0.5$, the stress-intensity factor is a minimum at the free surface and starts to increase to reach a maximum value at the maximum depth location. The maximum value of the normalized T-stress is near the free surface ($\phi \sim 5^{\circ}$) and decreases towards the maximum depth location ($\phi = 90^{\circ}$). The J-integral is a minimum value at the free surface and starts to increase towards the maximum depth location around the surface crack-front. Thus, the location along the surface-crack front where the product of a normalized J and T maximizes (assumed to be the critical fracture location) will be a function of both crack shape and crack size.

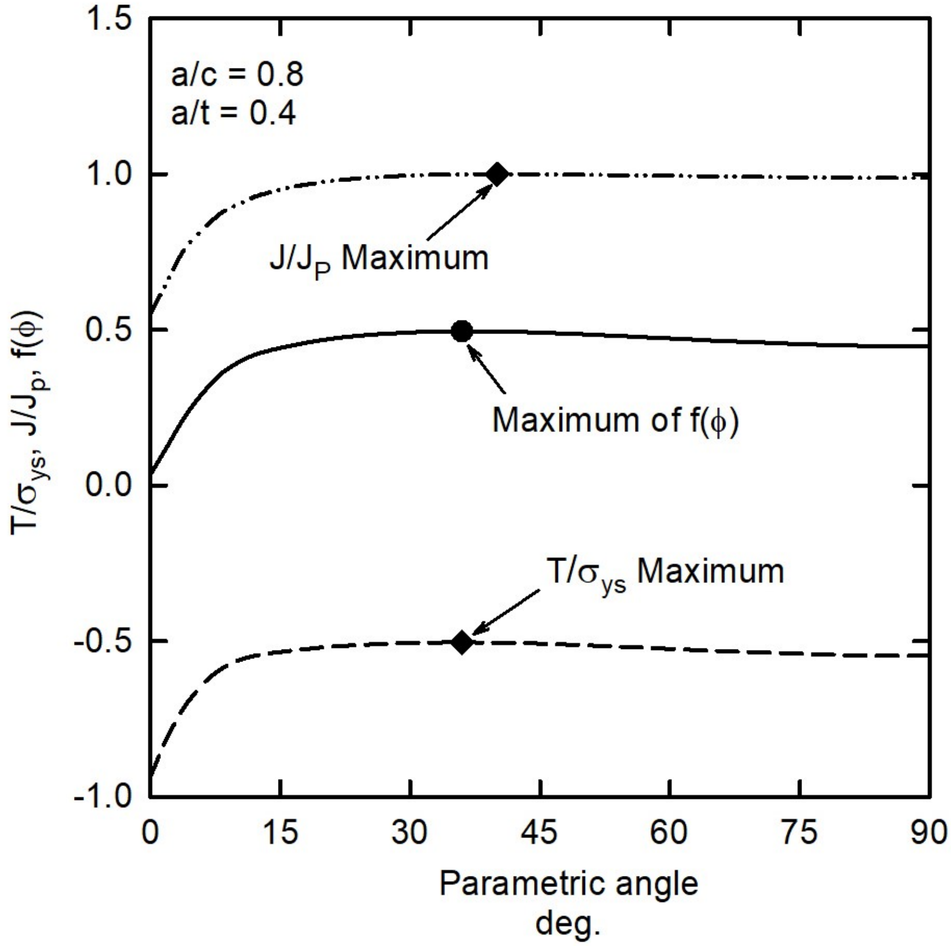

Figure 5.2 Example of predicting the critical angle using TASC software.

In this study, an equation for the critical parametric angle (ϕ_c) was developed for a wide range of crack-depth-to-crack-length (a/c) ratios and crack-depth-to-specimen-thickness (a/t) ratios. The equation was restricted to a/c values equal to or less than unity because of the limitation in the TASC software, only values of a/c ≤ 1.0 were analyzed. Table 5.1 shows the values of the critical parametric angle for different a/c and a/t and various strain-hardening coefficients (n) at a high-stress level. The applied stress level was selected to be high to model the fracture of surface cracks in ductile materials (S/σ_{ys} ~ 1.0).

From these results, it was concluded that the critical angles are weakly dependent on the strain-hardening coefficient (n). Thus, an averaged value for the critical parametric angle was chosen. It was concluded in this analysis that the critical parametric angle (ϕ_c) is independent of material properties.

Table 5.1 TASC critical parametric angles for different crack configurations and strain-hardening coefficients at a high stress level (S/σ_{ys} ~ 1.0).

a/c	a/t	ϕ_c, degree							Average. ϕ_c
		n=3	n=5	n=8	n=9	n=10	n=15	n=20	
0.2	0.2	88	88	88	88	88	88	88	88
	0.3	88	88	88	88	88	88	88	88
	0.4	88	88	88	88	88	88	88	88
	0.5	60	62	64	62	62	60	56	60.85
	0.6	50	50	46	46	44	42	40	45.42
	0.7	46	44	42	42	40	40	38	41.71
	0.8	40	36	34	34	34	32	30	34.28
0.6	0.2	50	86	86	86	86	86	86	80.85
	0.3	48	58	60	60	60	60	60	58
	0.4	42	42	40	40	40	38	38	40
	0.5	32	34	34	34	34	34	34	33.71
	0.6	32	32	32	32	32	32	30	31.71
	0.7	30	32	28	28	28	28	28	28.85
	0.8	26	26	26	26	26	26	26	26
1	0.2	60	60	60	46	46	44	44	51.42
	0.3	46	44	42	42	40	38	38	41.14
	0.4	34	32	32	32	34	34	34	33.14
	0.5	38	32	32	32	32	34	34	33.42
	0.6	30	30	30	30	30	30	30	30
	0.7	30	28	28	28	28	28	28	28.28
	0.8	26	26	26	26	26	26	26	26

An equation for the critical parametric angle was developed as a function of a/c and a/t, which is simpler than using equations 5.3 that was used in the TASC software. The equation is independent of material properties (n, σ_{ys}, E). For a/c ≤ 1, the equation is

$$\phi_c = \phi_o + A\left\{\cos\left[90\left(\frac{a}{t}\right)\right]\right\}^p \tag{5.4}$$

where:

$$\phi_o = 30 - 5\left(\frac{a}{c}\right) \tag{5.5}$$

$$A = 60 - 30\left(\frac{a}{c}\right)^2 \tag{5.6}$$

and,

$$p = 1.3 + 3.5\left(\frac{a}{c}\right) \tag{5.7}$$

Figure 5.3 shows how the critical parameter angles from TASC software (symbols) vary with the strain-hardening coefficient for a semi-circular surface crack as a function of a/t. The solid curve is equation 5.4, which fits the TASC results fairly well. It would have been of interest if the TASC software had analyses for a/t less than 0.2, to see if the critical angles would have been along the crack front at about 50 to 60 degrees, or elsewhere. For a/t < 0.2, the stress-intensity factor is about 12% higher at the free surface ($\phi = 0$) than at the maximum depth location ($\phi = 90$ deg.). The free-surface location has much lower constraint (herein normalized T stress) than the maximum depth location. Thus, it is expected on the basis of J and constraint that the critical location would be about mid-way along the crack front.

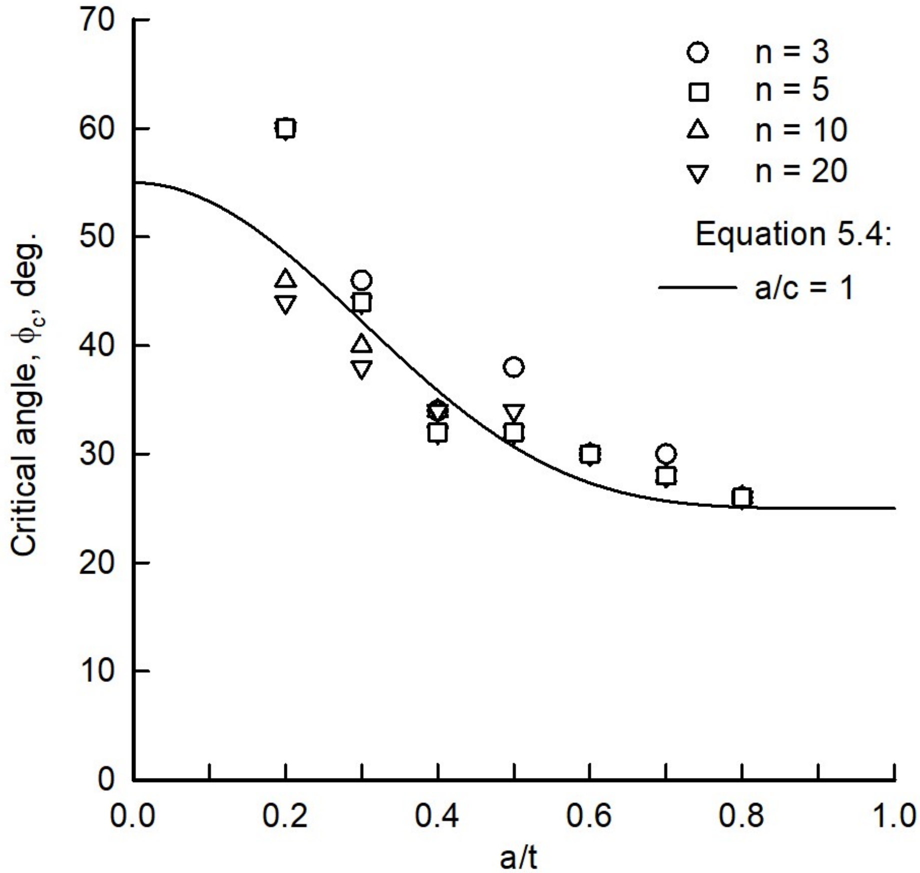

Figure 5.3 Critical parametric angle for a/c = 1 and various a/t ratios for various strain hardening values.

A plot of equation 5.4 and the TASC critical angles for different crack configurations are given in Figure 5.4. In general, the TASC critical angles are close to the proposed equation for different crack configurations. However, some crack configurations need to be further analyzed. In the next section, some of these cases that are far from the curves will be analyzed in detail.

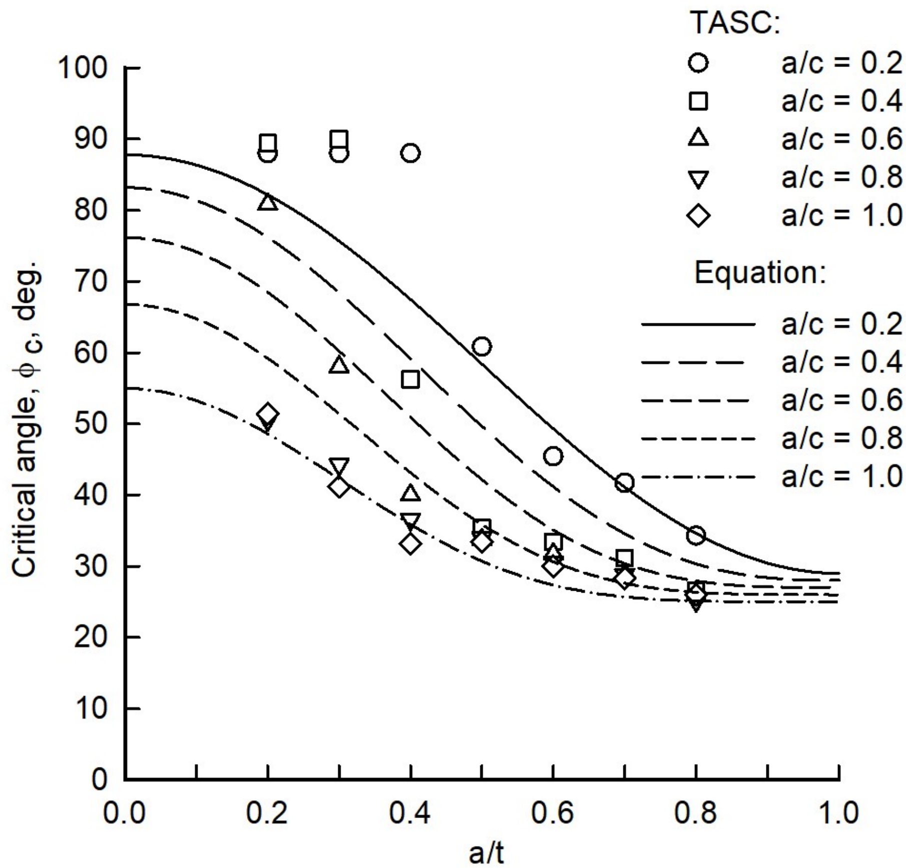

Figure 5.4 Critical parametric angle equation and TASC angles for different crack configurations.

5.2 Comparison of critical angles for various crack configurations

A critical angle equation was developed using the data from the NASA TASC software for different crack shapes and sizes, but an analysis was done herein for certain cases that show significantly large differences in the critical angles. Figure 5.5 shows some of the cases that have large differences between TASC values and the proposed equation. These cases, shown as solid symbols, are evaluated herein.

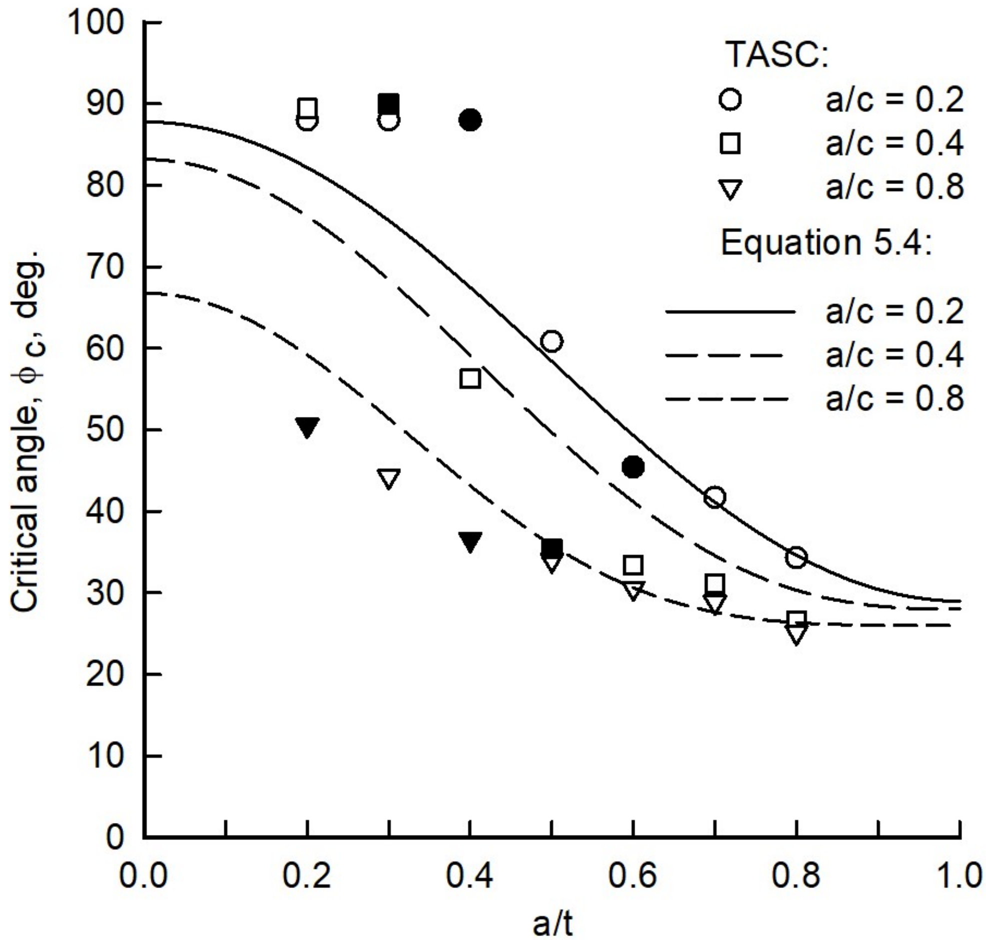

Figure 5.5 Critical parametric angle equation and TASC values for different crack configurations that show large differences in angles.

In order to verify the output results from the TASC software with the proposed equation, plots of equation 5.3 given by Allen and Wells [14, 15] have been used with the proposed equation (5.4) to see if there are large differences between the calculated values of the critical stress-intensity factor at failure using either the TASC angle or the angle from the proposed equation. Thus, the Newman-Raju boundary-correction factor (F_{NR}) was also added to the plots. Figures (5.6) to (5.11) show the fracture parameter plots for six different crack configurations. They are: (1) a/c = 0.2 with a/t = 0.4 or 0.6, (2) a/c = 0.4 with a/t = 0.3 or 0.5, and (3) a/c = 0.8 with a/t = 0.2 or 0.4.

From the plots, it can be noticed that the cases for large differences between the TASC angles and the proposed equation (5.4) angles, the differences between the critical stress-intensity boundary-correction factors (F_{NR}) at these two angles are negligible (generally less than 6.5%). Therefore, equation 5.4 can be used for a/c < 1 instead of equation 5.3 due to its simplicity, since it is only dependent on crack shapes and sizes.

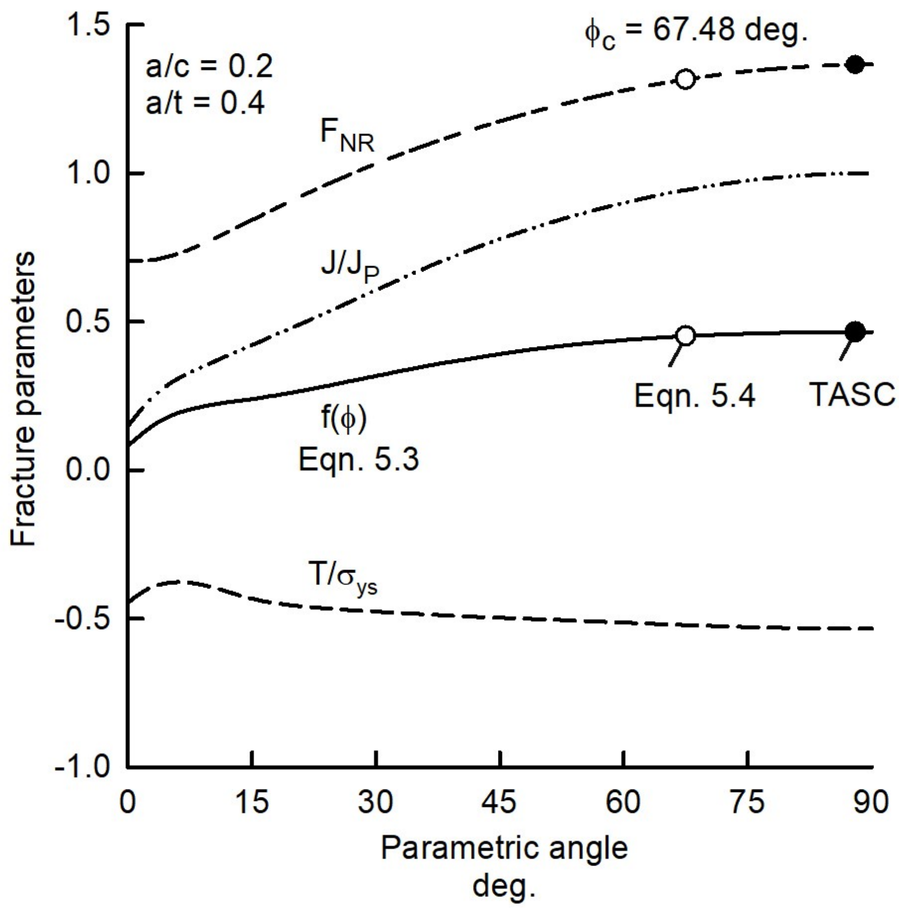

Figure 5.6 Determination of critical angle for a/c= 0.2 and a/t= 0.4.

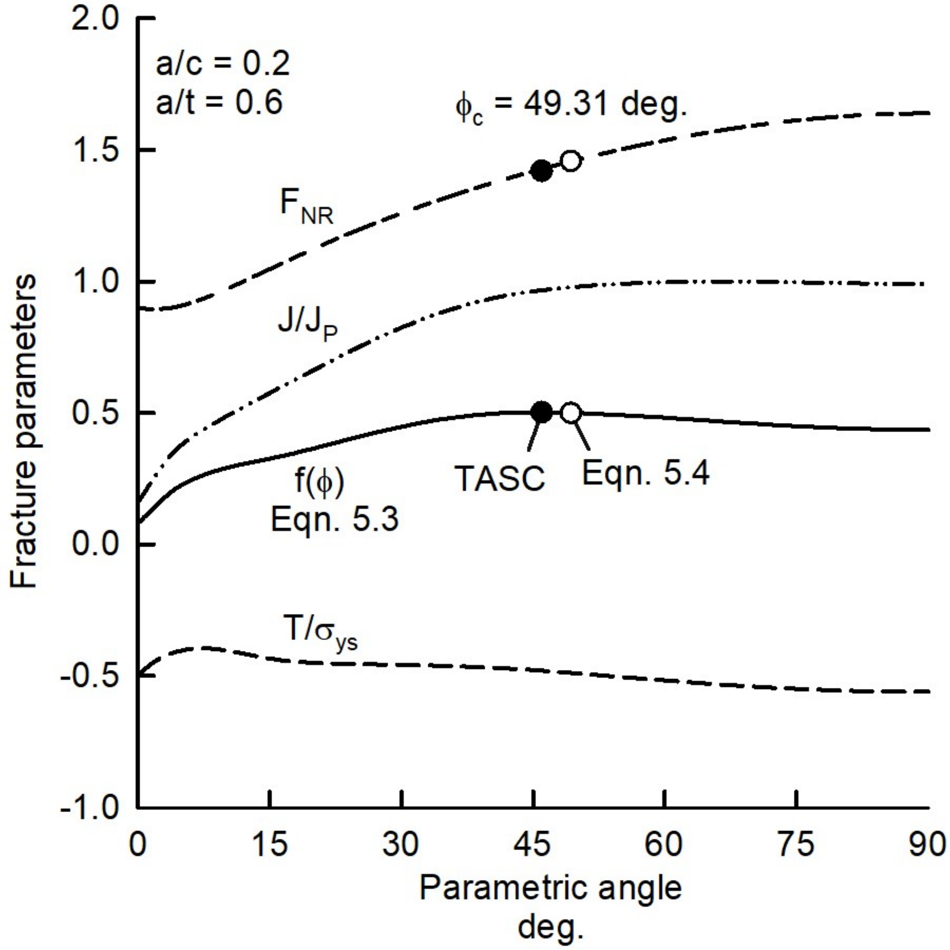

Figure 5.7 Determination of critical angle for a/c= 0.2 and a/t= 0.6.

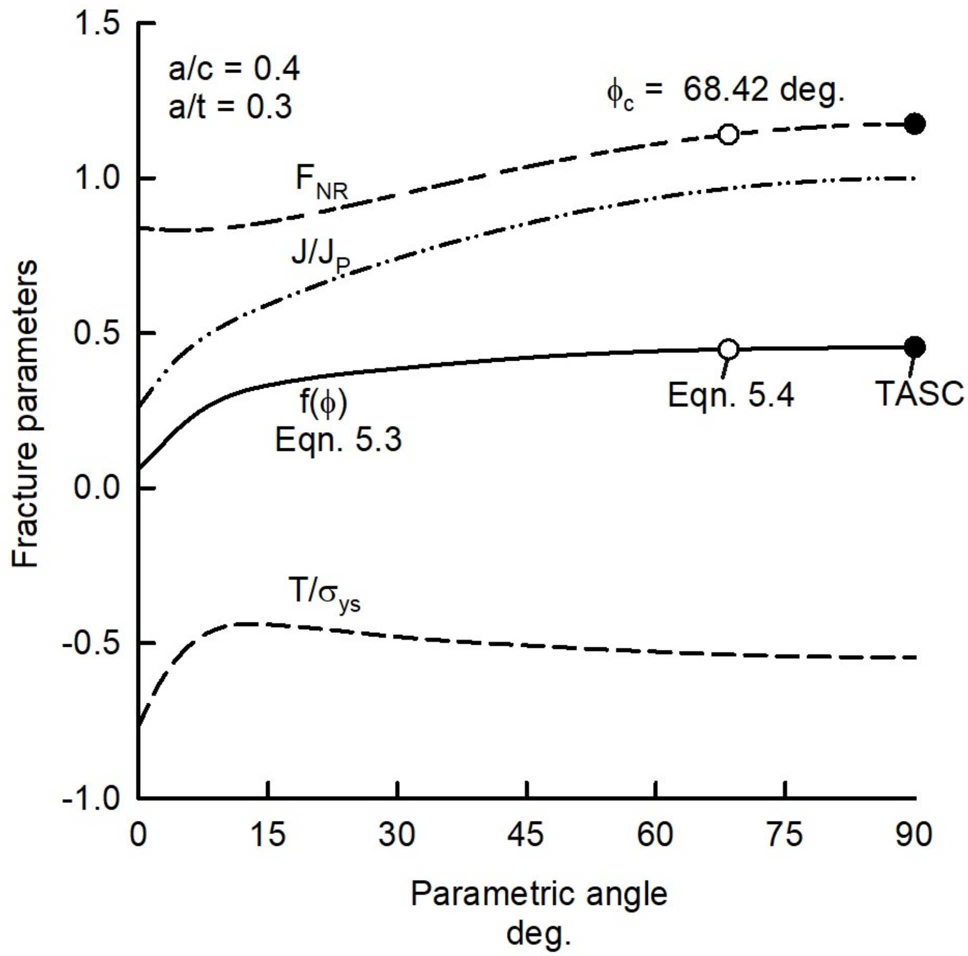

Figure 5.8 Determination of critical angle for a/c= 0.4 and a/t= 0.3.

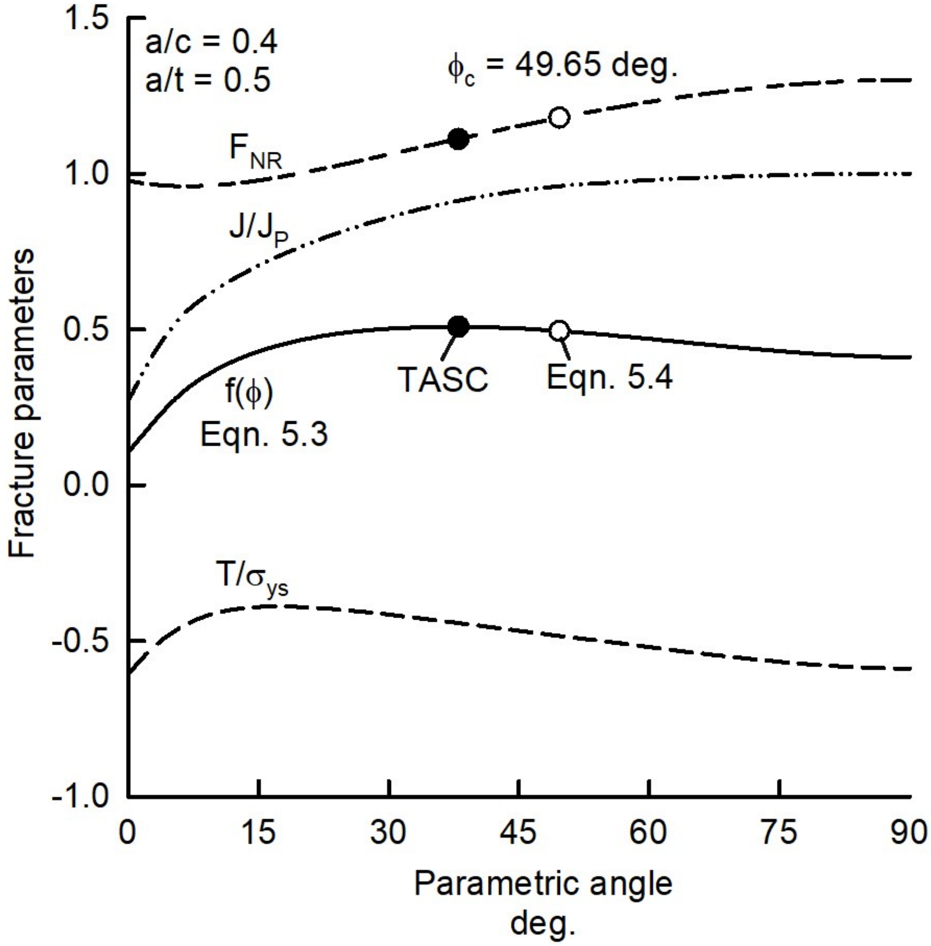

Figure 5.9 Determination of critical angle for a/c= 0.4 and a/t= 0.5.

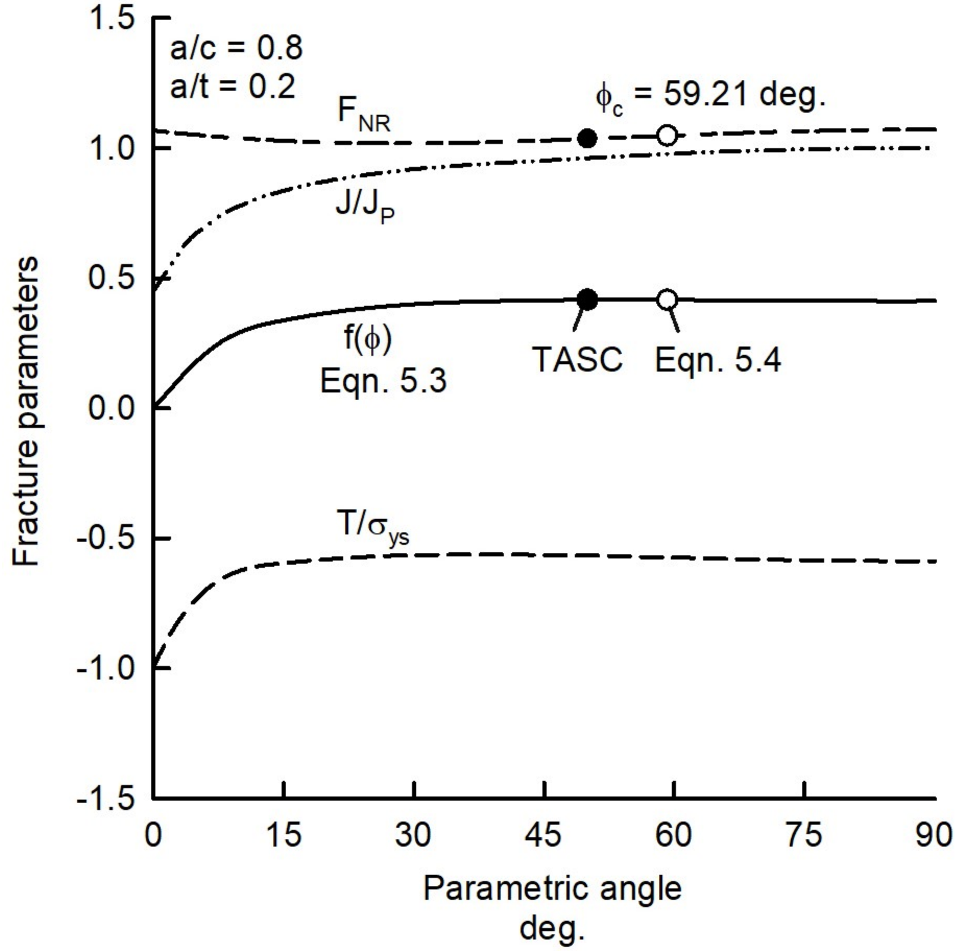

Figure 5.10 Determination of critical angle for a/c= 0.8 and a/t= 0.2.

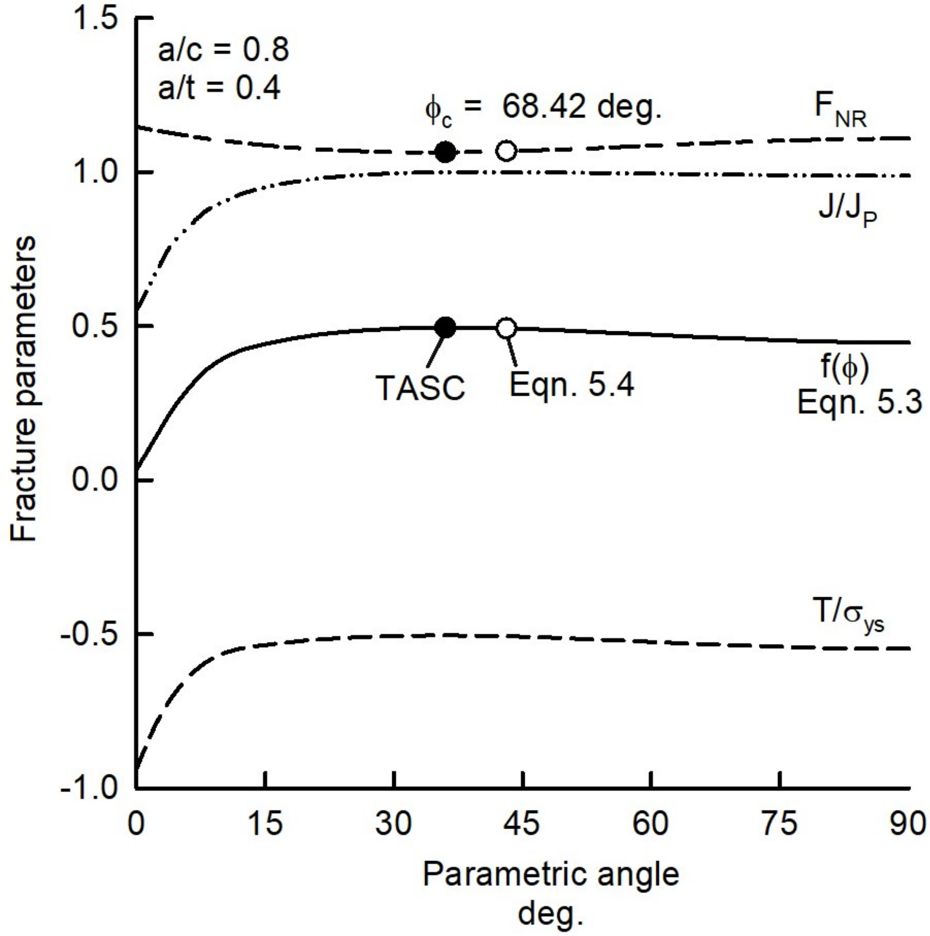

Figure 5.11 Determination of critical angle for a/c= 0.8 and a/t= 0.4.

All of the previous analyses were done for a high-applied stress level for application to surface cracks in ductile materials. The proposed equation (5.4) was developed for high-applied stress levels.

The calculated critical parametric angle from the TASC software using equation (5.3) changes as a function of crack shape and crack size with increasing applied stress level. An evaluation of the variation of the critical parametric angle with respect to applied stress level was conducted for various crack shapes (a/c) and sizes (a/t). Because the proposed equation (5.4) is nearly independent of strain-hardening coefficient, n = 9 was chosen for this analysis.

Figures 5.12 to 5.16 show the variation of the critical parametric angle against the applied stress level for different crack configurations, $0.2 \leq a/c \leq 1.0$ and $0.2 \leq a/t \leq 0.8$. The solid symbols represent the critical parametric angles for high applied stress levels that were used to develop equation (5.4).

From the plots, it can be noticed that there is a significant difference on the critical parametric angle with respect to the applied stress level, which may impact the calculation of the critical stress-intensity factor.

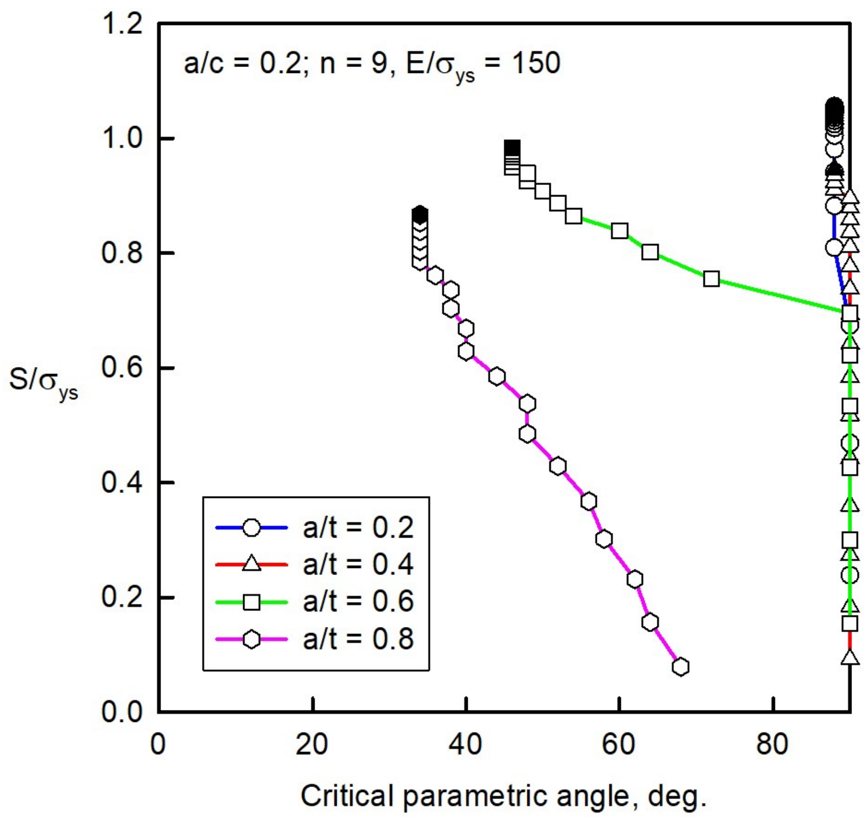

Figure 5.12 Variation of critical parametric angle against stress level for a/c = 0.2 and different a/t.

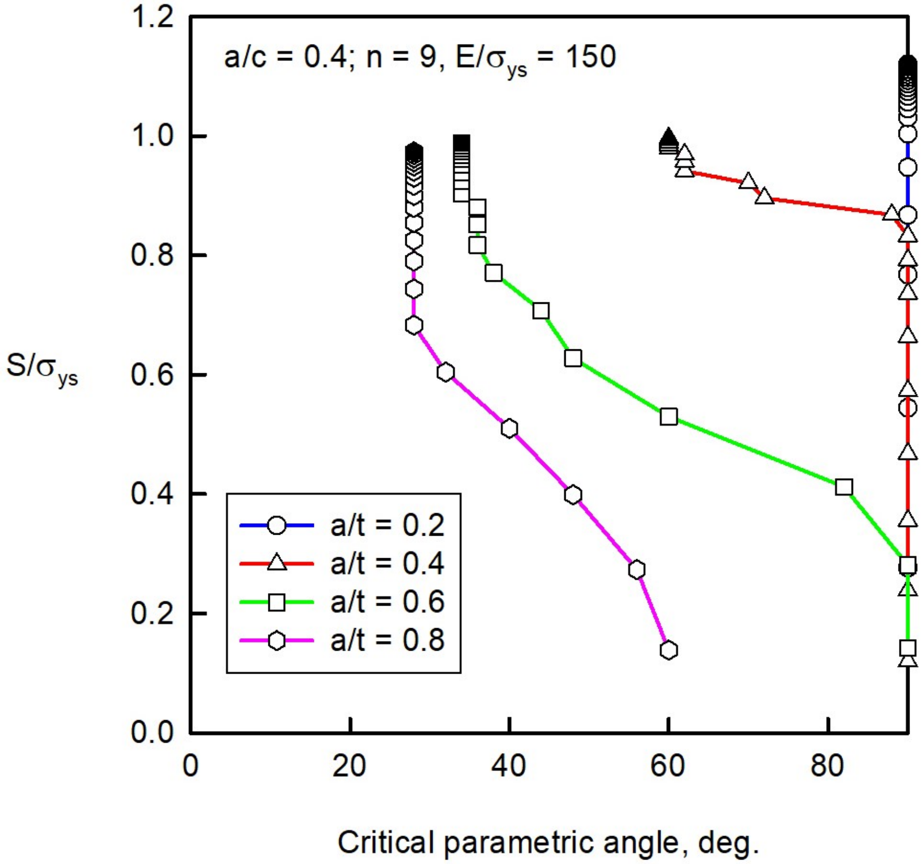

Figure 5.13 Variation of critical parametric angle against stress level for a/c = 0.4 and different a/t.

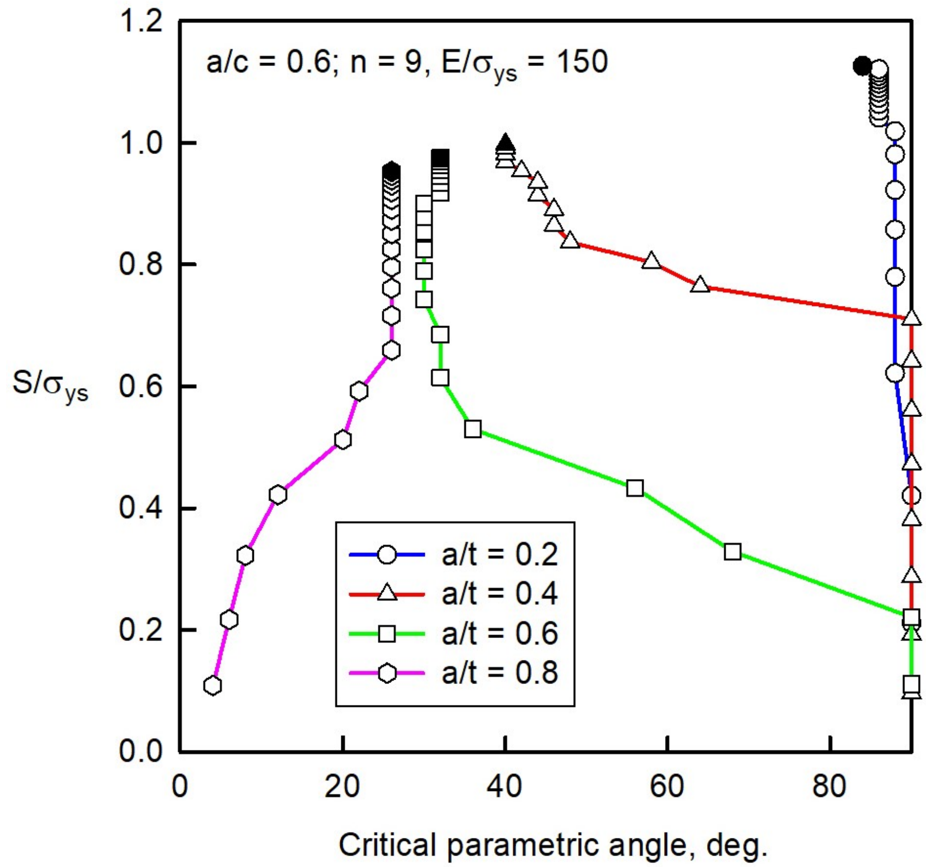

Figure 5.14 Variation of critical parametric angle against stress level for a/c = 0.6 and different a/t.

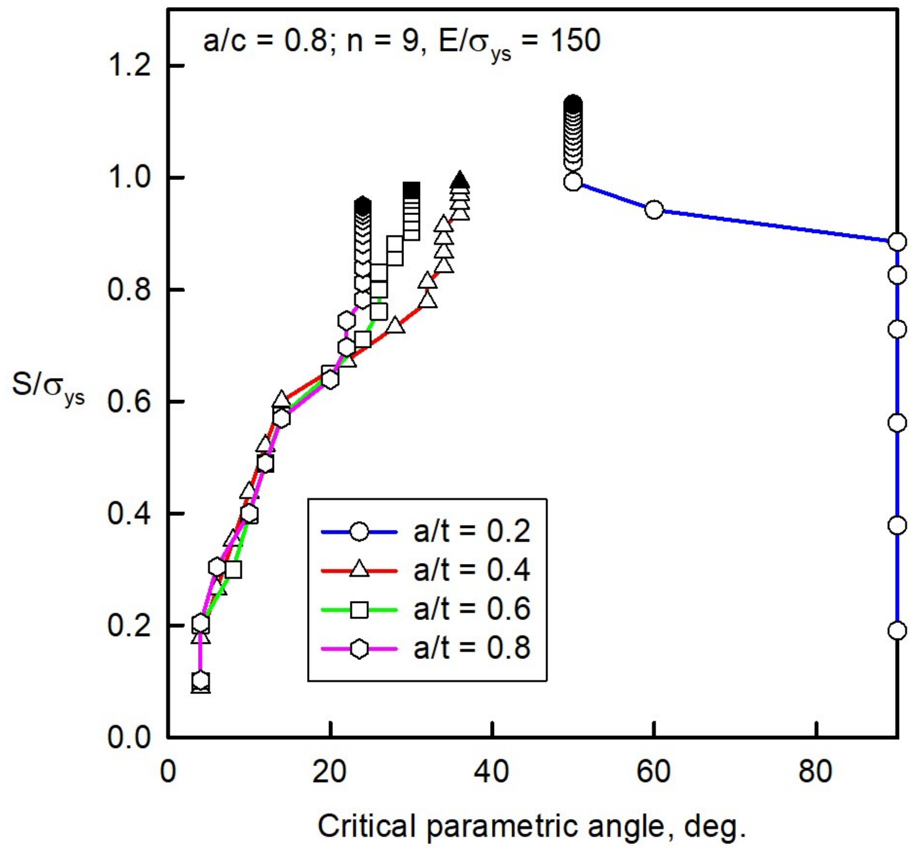

Figure 5.15 Variation of critical parametric angle against stress level for a/c = 0.8 and different a/t.

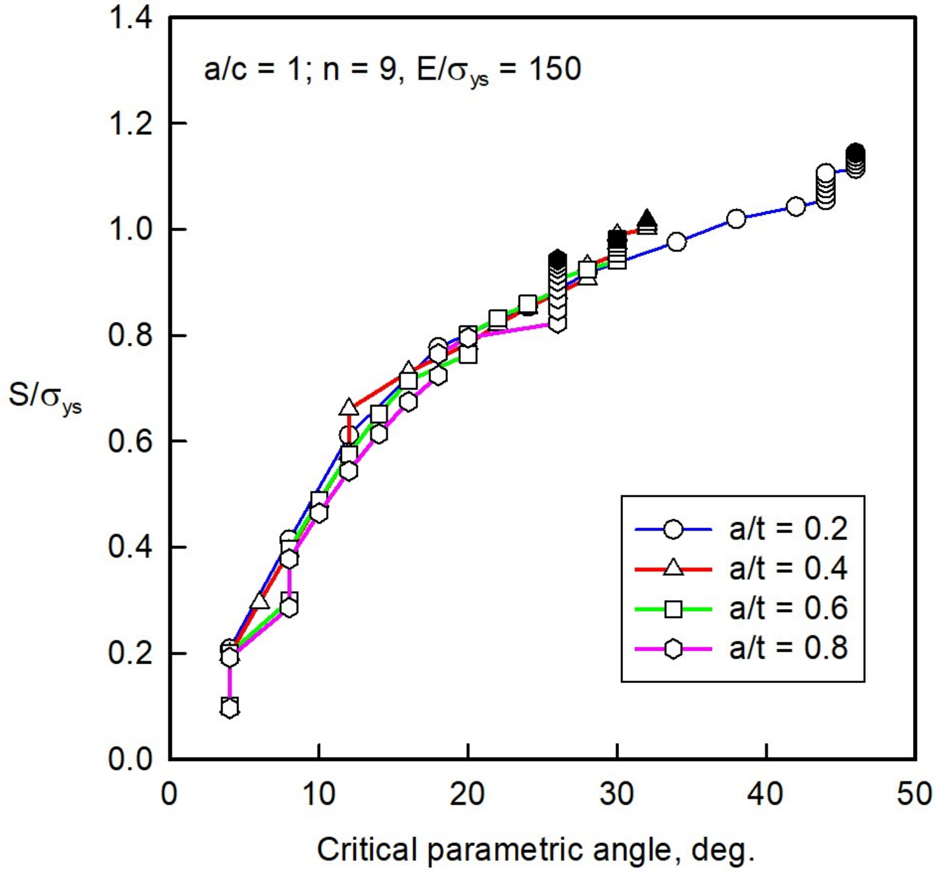

Figure 5.16 Variation of critical parametric angle against stress level for a/c = 1.0 and different a/t.

CHAPTER VI

FRACTURE ANALYSIS USING TPFC AND CRITICAL ANGLES

A fracture analysis was done for the three materials (Ti-6Al-6V-2Sn, Ti-6Al-4V titanium alloys and 301 stainless steel) tested by Smith [16] using the Two-Parameter Fracture Criterion (TPFC). In the TPFC, the Newman-Raju stress-intensity factor equation [8] and the proposed critical angle equation (5.4) was used to calculate the critical stress-intensity factors at failure (K_{Ie}). From the net-section failure stresses (S_n), tensile properties, and K_{Ie}, the two fracture parameters (K_F and m) were determined.

For each material, three plots were made during these analyses. The first plot shows the variation of critical K_{Ie} with respect to the net-stress-to-ultimate-strength (S_n/σ_u) ratio, where the two parameters K_F and m were generated using a least-squares method. The second plot shows the variation of S_n/σ_u with respect to a crack-tip parameter ($c_i\, F_n^2$), and the last plot shows the variation of K_{Ie} with respect to the crack-tip parameter.

6.1 Ti-6Al-6V-2Sn titanium alloy

The surface-crack fracture data for the Ti-6Al-6V-2Sn alloy [16] are given in Tables 2.3 and 2.4 for longitudinal and transverse directions, respectively. Since there is very little difference in both the yield and ultimate tensile strength between the longitudinal and transverse directions, the two data sets were analyzed together. Using the proposed critical angle equation and the Newman-Raju K equation, the K_{Ie} values are shown in Figure 6.1 as a function of S_n normalized by the ultimate strength. The square symbols are for specimens in the transverse direction and circle symbols are for the longitudinal direction. A least-squares fit of the TPFC would have resulted in a *negative* value of the fracture-ductility parameter, m, because of the two test results at the highest net-section stress. The physical range of m (slope on a K_{Ie} against S_n/σ_u plot) is between 0 and 1. Thus, m was set equal to zero and the K_{Ie} values were then averaged to determine K_F (32 MPa-m$^{1/2}$). Thus, this alloy is a high-strength and low-toughness titanium alloy; and LEFM procedures are able to correlate and predict failures for a wide range in surface-crack configurations.

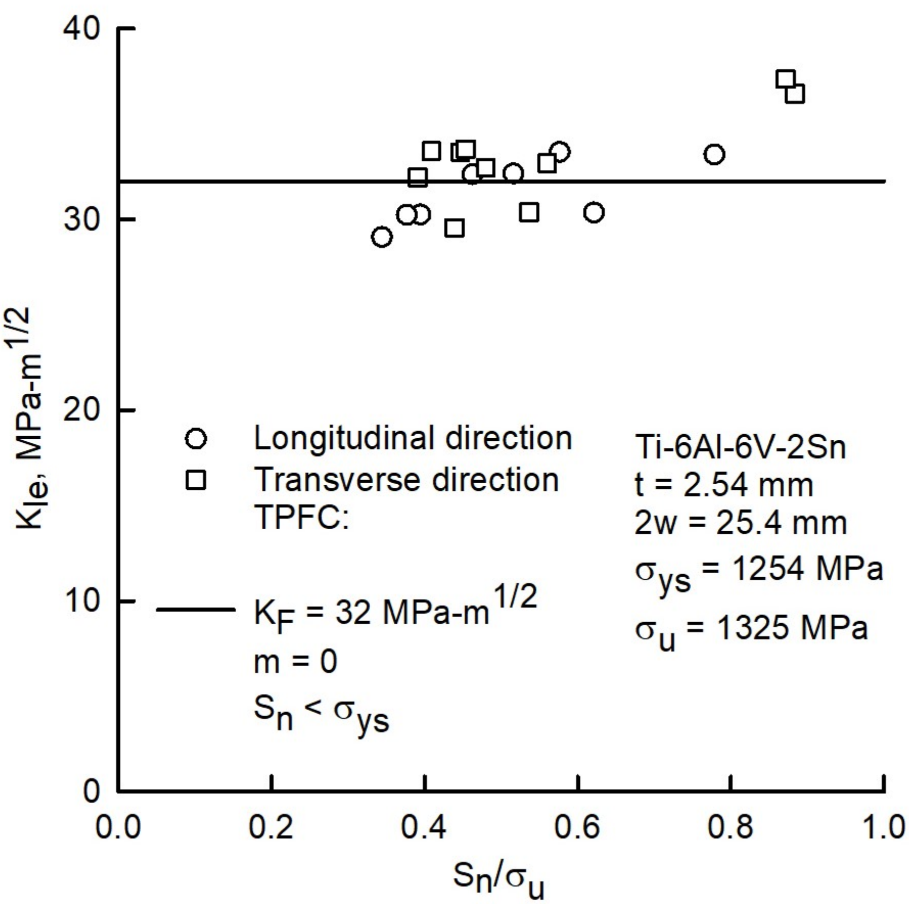

Figure 6.1 Critical stress-intensity factor against net-section-stress-to-ultimate-strength ratio at failure for Ti-6Al-6V-2Sn.

When m is equal to zero, the TPFC equation 4.4 reduces to the LEFM stress-intensity factor K_{Ie} is equal to K_F. The fracture data correlated very well (within ±10%) for most cases with $0.44 \leq a/c \leq 0.76$ and $0.2 \leq a/t \leq 0.63$ for tests in the longitudinal direction and $0.39 \leq a/c \leq 0.69$ and $0.2 \leq a/t \leq 0.6$ for those in the transverse direction. But the two tests at the highest value of net-section stress produced exceptionally high values of K_{Ie}. These specimens failed at K_{Ie} = 36.6 and 37.4 MPa-$m^{1/2}$, respectively, which are 14% and 17% higher than the average fracture toughness. The critical parametric angles for the fracture data ranged from 38˚ to 65˚ for specimens in the longitudinal direction, and 36˚ to 68˚ for specimens in the transverse direction.

Figure 6.2 shows a plot of net-section stress normalized by the ultimate strength (S_n/σ_u) ratio with respect to the crack-tip parameter ($c_i F_n^2$). F_n is the net-section boundary-correction factor and was derived earlier (eqn. 3.30). The TPFC equation indicates that the net-section stress at failure is unique with respect to the crack-tip parameter, so if different surface-crack configurations (different a/c and a/t) have the same $c_i F_n^2$, then S_n is the same. The TPFC equation (solid curve) correlated the fracture data very well. The dashed line is $S_n = \sigma_u$.

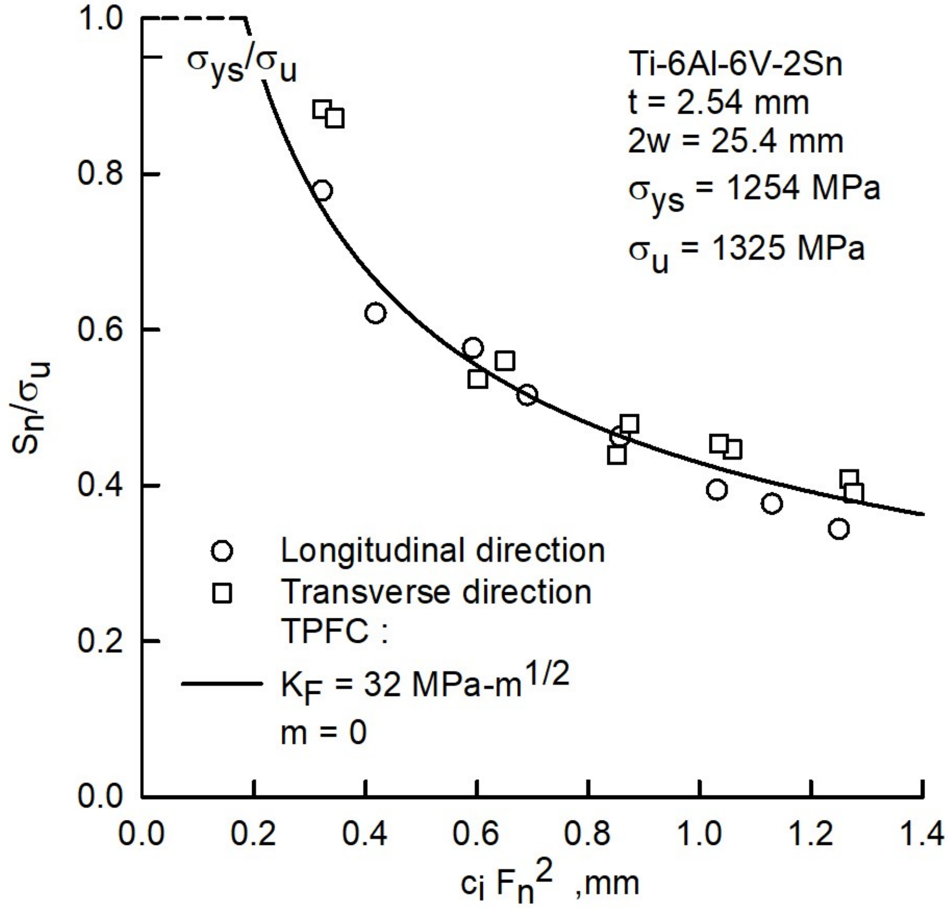

Figure 6.2 Net-section stress at failure normalized by ultimate strength against crack-tip parameter for Ti-6Al-6V-2Sn.

Figure 6.3 illustrates the variation of the critical stress-intensity factor at failure (K_{Ie}) against the crack-tip parameter for different crack configurations. Since m = 0 the TPFC equation is represented by the horizontal line. About 80% of the fracture tests correlated within about ±5%, which is very good. But the maximum error was about 15%.

The proposed equation 5.4 was developed using high-stress-level data from the TASC software, meaning that the equation was developed for ductile materials. However, the Ti-6Al-6V-2Sn titanium alloy is a very brittle alloy. But using the proposed equation, the fracture data correlated very well using the TPFC (m = 0).

For very brittle materials, the maximum stress-intensity factor should be used to analyze the fracture data. Figure 6.4 used the parametric angle associated with the maximum value from the Newman-Raju boundary-correction factor F_{NR}. The fracture tests correlated very well and were within ±10%. The fracture test data correlated slightly better using the maximum stress-intensity factors than those predicted using equation 5.4.

In conclusion, the fracture data for the Ti-6Al-6V-2Sn brittle titanium alloy were in accordance with the TPFC; and the fracture analyses showed that the TPFC can be successfully applied to this material. Thus, it appears that equation 5.4 can be used for brittle materials, but further studies on other brittle materials would be useful.

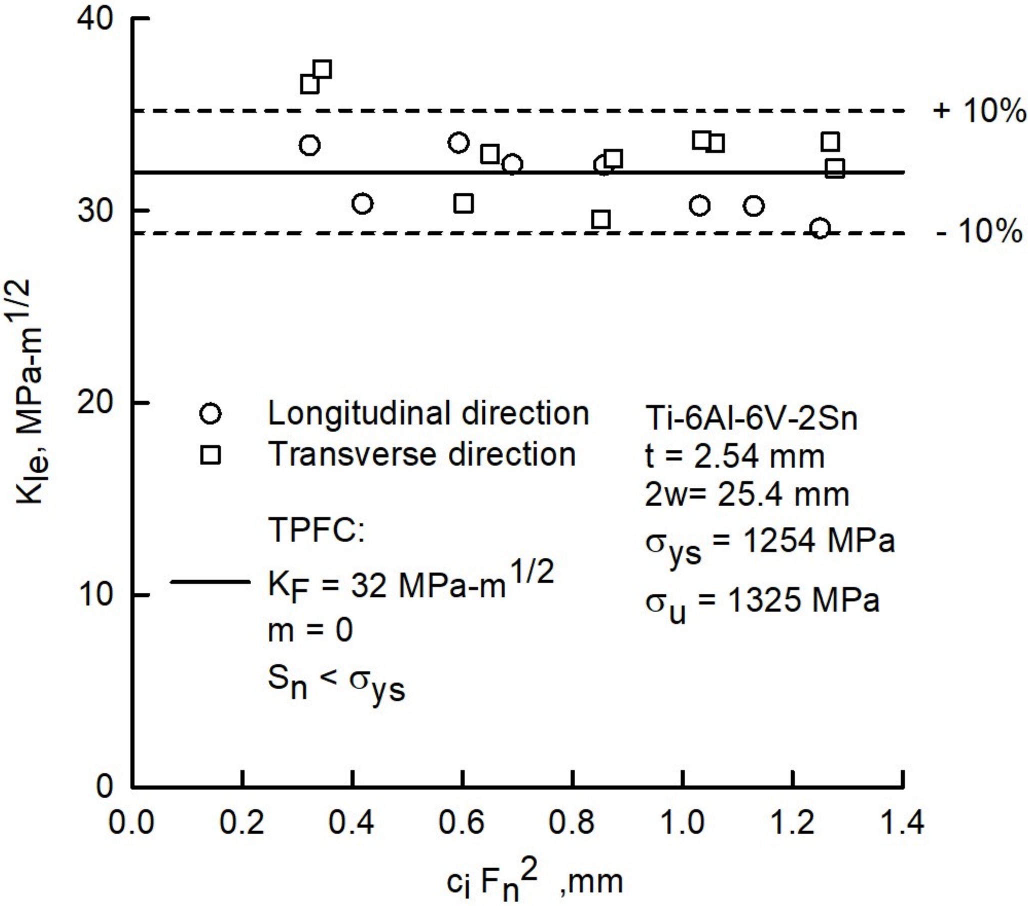

Figure 6.3 Critical stress-intensity factor at failure against crack-tip parameter for Ti-6Al-6V-2Sn.

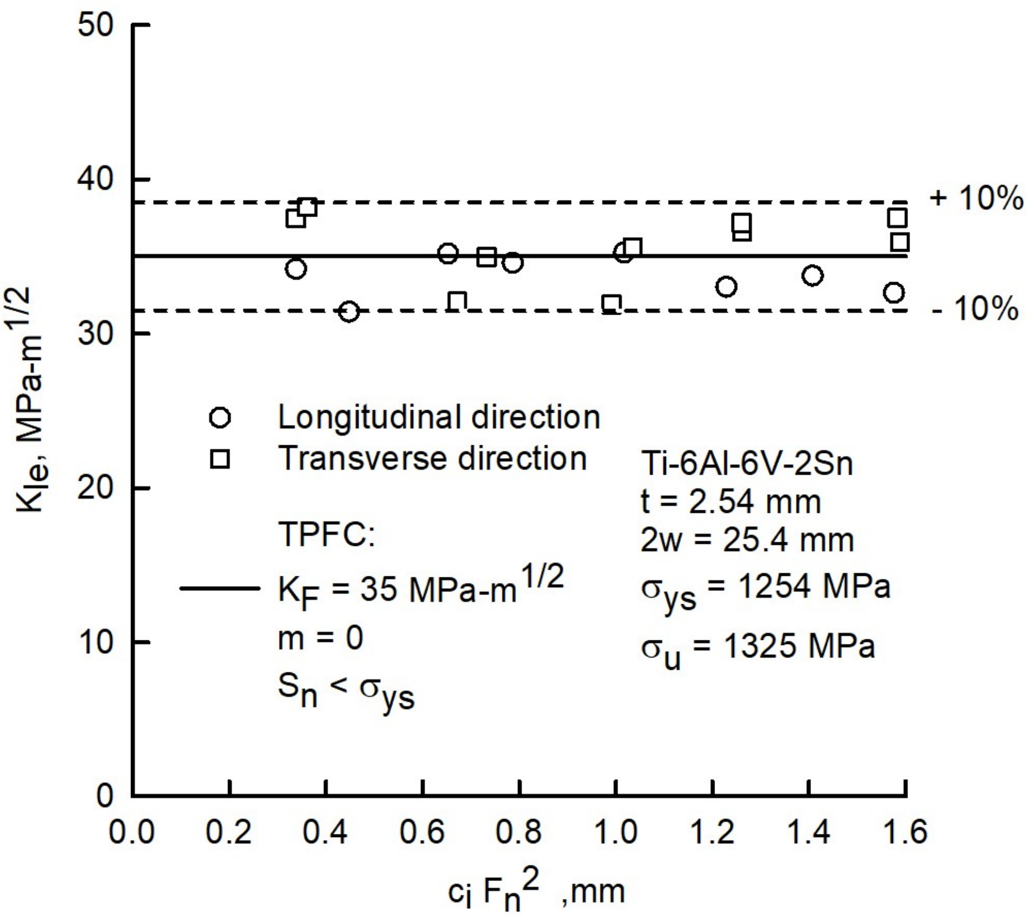

Figure 6.4 Critical stress-intensity factor at failure against crack-tip parameter for Ti-6Al-6V-2Sn using F_{NR} maximum.

6.2 Ti-6Al-4V titanium alloy

The Ti-6Al-4V titanium alloy is similar to Ti-6Al-6V-2Sn in many ways and but has a significantly lower strength level, and exhibits more ductility. The surface-crack fracture data for the Ti-6Al-4V alloy [16] are given in Tables 2.7 and 2.8 for longitudinal and transverse directions, respectively. Again, since there is very little difference in both the yield stress and ultimate tensile strength between the longitudinal and transverse directions, the two data sets were analyzed together. Using the proposed critical angle equation and the Newman-Raju K equation, the K_{Ie} values are shown in Figure 6.5 as a function of S_n normalized by the ultimate strength. The circular symbols are for specimens in the longitudinal direction and square symbols are for the transverse direction. Because most of the fracture data has S_n greater than the yield stress, a least-squares fit was made using equation 4.6, instead of equation 4.5. The best-fit procedure gave K_F = 178 MPa-$m^{1/2}$ and m = 0.71. In contrast to the Ti-6Al-6V-2Sn, which was very brittle, the Ti-6Al-4V alloy has much higher fracture toughness and is very ductile. The solid line is equation 4.5 using the values of K_F and m. And the vertical dashed line is the ultimate tensile strength. One has to notice that there are some data points that failed at $Sn > \sigma_u$. These failures were caused by crack strengthening, as pointed out by Newman [7, 23]. Crack strengthening is caused by the tri-axial stress state along the un-cracked ligament (net-section) and the flow stress is elevated due to the von Mises yield criterion. The correlation of the fracture data was within ±3%.

The fracture data correlated very well with the TPFC for both $S_n > \sigma_{ys}$ and $S_n < \sigma_{ys}$. The critical parametric angle for the fracture data ranged from $40^\circ \leq \phi_c \leq 85^\circ$ for specimens in the longitudinal direction and $33^\circ \leq \phi_c \leq 64^\circ$ for specimens in the transverse direction. The critical stress-intensity factor at failure ranged from, $23 \leq K_{Ie} \leq 64$ MPa-$m^{1/2}$ and $33.5 \leq K_{Ie} \leq 64$ MPa-$m^{1/2}$ for both longitudinal and transverse directions, respectively.

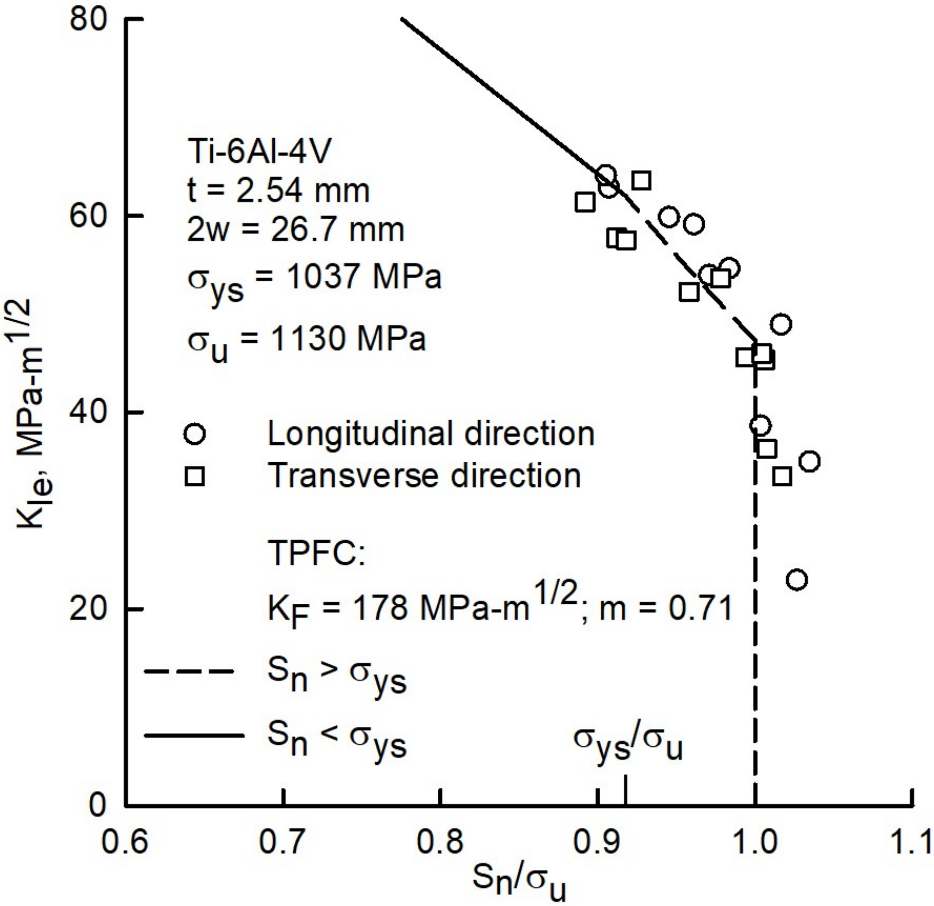

Figure 6.5 Critical stress-intensity factor versus net-section-stress-to-ultimate-strength ratio at failure for Ti-6Al-4V.

Figures 6.6 and 6.7 shows the behavior of the net-section stress normalized by the ultimate strength (S_n/σ_u) and the K_{Ie}values, respectively, against the crack-tip parameter ($c_i F_n^2$), as for the Ti-6Al-4V alloy. In both cases, the TPFC matched the fracture data very well (within ±3%). For $S_n = \sigma_u$, an equation was used [23] to find the TPFC curve:

$$K_{Ie} = \sigma_u \sqrt{\pi c_i}\, F_n \tag{6.1}$$

In conclusion, the fracture data for the Ti-6Al-4V titanium alloy correlated very well with the TPFC and matched the previous analysis (not shown) that had been conducted by Newman [7] using an engineering estimate for the critical parameter angles.

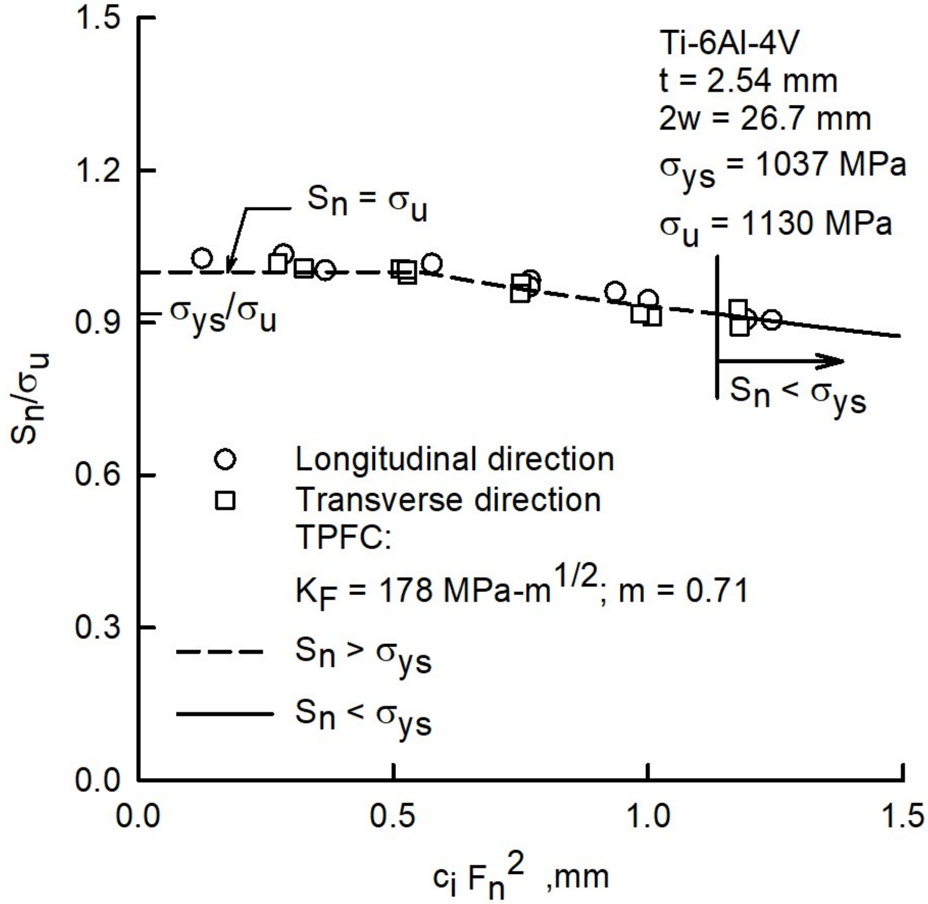

Figure 6.6 Net-section stress at failure normalized by ultimate strength against crack-tip parameter for Ti-6Al-4V.

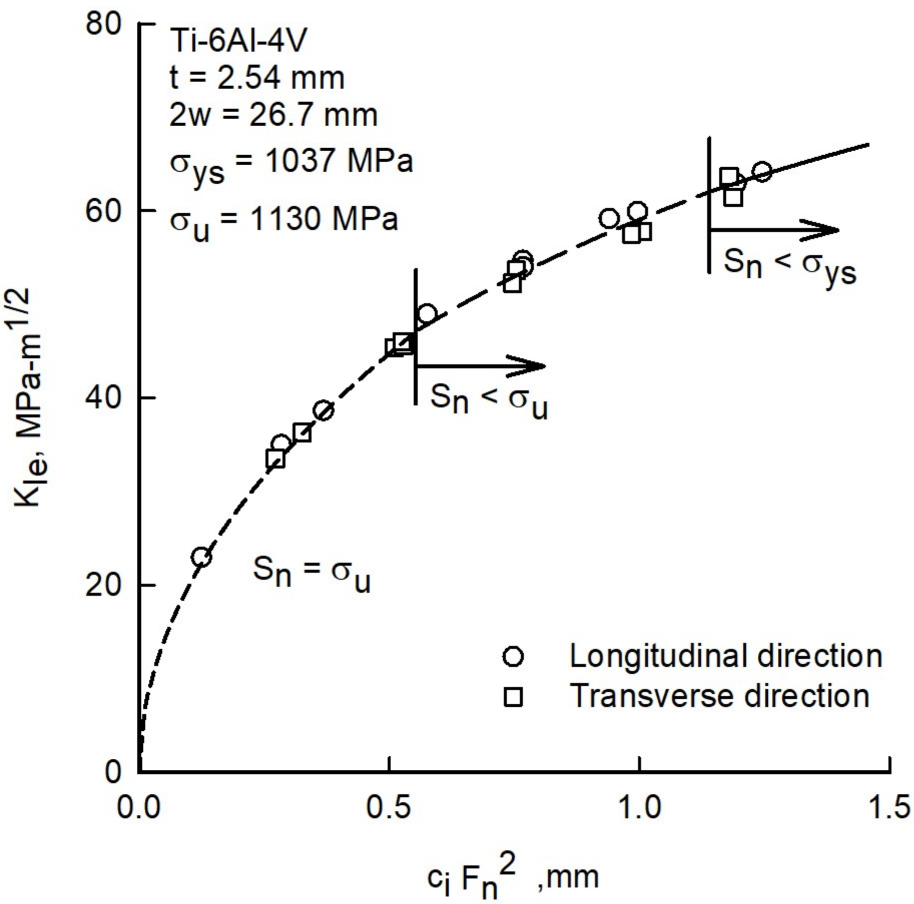

Figure 6.7 Critical stress-intensity factor at failure against crack-tip parameter for Ti-6Al-4V.

6.3 Ardeformed 301 stainless steel

The 301 stainless steel is well known for its high-strength properties and ductility. The surface-crack fracture data generated by Smith [16] on the 301 steel are shown in Tables 2.10 to 2.12. He had tested three steels that had different heat and processing treatments and had three different strength levels. They have been denoted as steels A, B and C. Steel A and B are the highest strength materials and steel C has the lowest strength. In the TPFC analyses, steels A and B have been combined (strength levels were less than 4% different), while steel C was analyzed separately. Steel C has a strength level that was 16% lower than steel A.

Figure 6.8 illustrates the behaviour of the critical stress-intensity factors at failure (K_{Ie}) against the net-section stress to ultimate strength ratio for the three different steels analyzed. A TPFC analysis was conducted on the three materials. Since the ultimate and yield strength for both steels A and B were close to each other (see Table 2.9), an average value of K_F and m were used. Analyses on steels A and B gave K_F = 460 MPa-$m^{1/2}$ and m = 0.8. On the other hand, steel C showed less strength and gave a lower fracture toughness, K_F = 380 MPa-$m^{1/2}$ with m=0.8. (Note that these three steels have very little strain hardening. The yield stress and ultimate tensile strength are very close to each other. Thus, the TPFC equation 4.6 was not used, only equation 4.5 was used to calculate the K_{Ie} values.) Again, there was some evidence of crack strengthening on steels A and B, but not on steel C. A wide range of surface-crack configurations were analyzed for the three steels. For all three steels, the critical parametric angles ranged from 30˚ to 52˚.

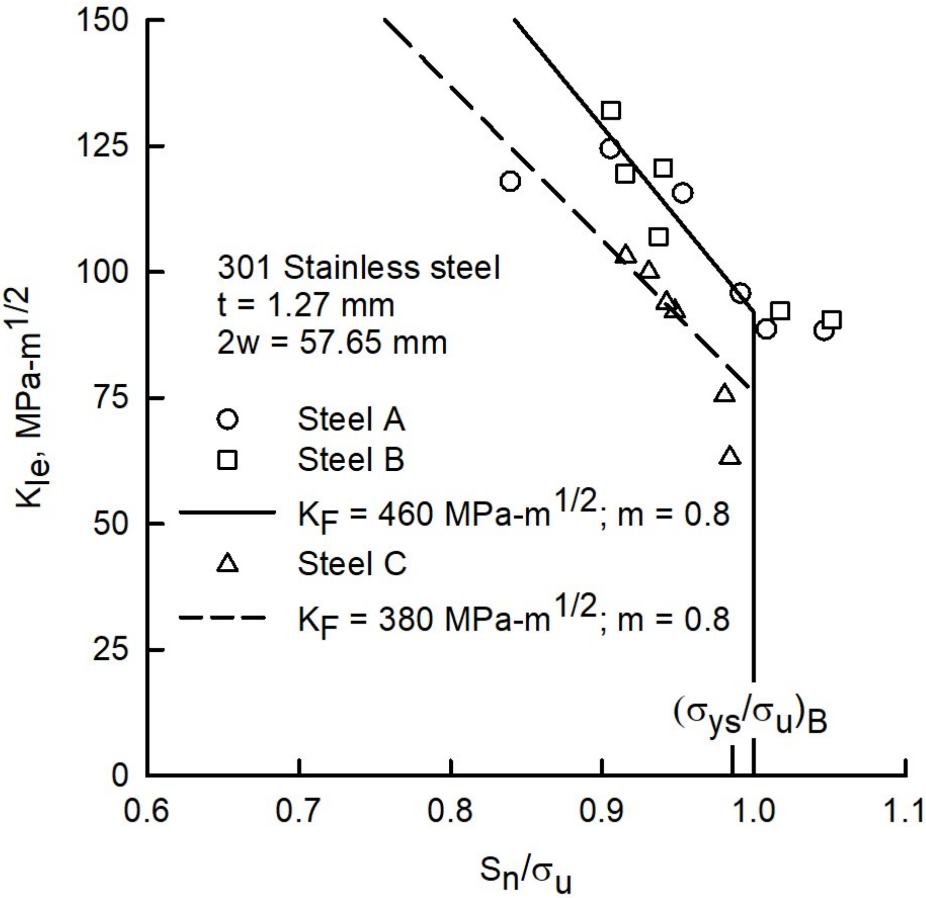

Figure 6.8 Critical stress-intensity factor against net-section-stress-to-ultimate strength ratio at failure for Ardeformed 301 stainless steel.

Figure 6.9 shows the variation of S_n/σ_u against the crack-tip parameter ($c_iF_n^2$) for various crack configurations. The ultimate tensile strength of the respective material (A, B or C) was used the normalization. The TPFC (solid curve) correlated the fracture data on steels A and B very well (within ±5%). And more than 80% of the fracture test data correlated within 3%. While the TPFC (dashed curve) correlated the fracture data on steel C within 1%. Steel C had a lower strength and lower fracture toughness in comparison to steels A and B, but the failure stresses were essentially the same. However, more variation is shown in the K_{Ie} against crack-tip parameter results, shown in Figure 6.10, which indicates that K_{Ie} is more sensitive to the strength level and fracture toughness values.

Figure 6.10 illustrates how K_{Ie} varies against the crack-tip parameter. It is noticed that steels A and B have the highest strength levels and they have higher critical stress-intensity factors at failure than steel C. Since the ultimate tensile strength was almost equal to the yield stress for all of these steels, the equation for $S_n > \sigma_{ys}$ was not used; and equation (6.1), where $S_n = \sigma_u$, was used for small values of the crack-tip parameter. The solid curve are K_{Ie} values calculated from the TPFC for net-section stresses less than the yield stress of the respective material; and the dashed curves are K_{Ie} values calculated with the ultimate tensile strength of each material.

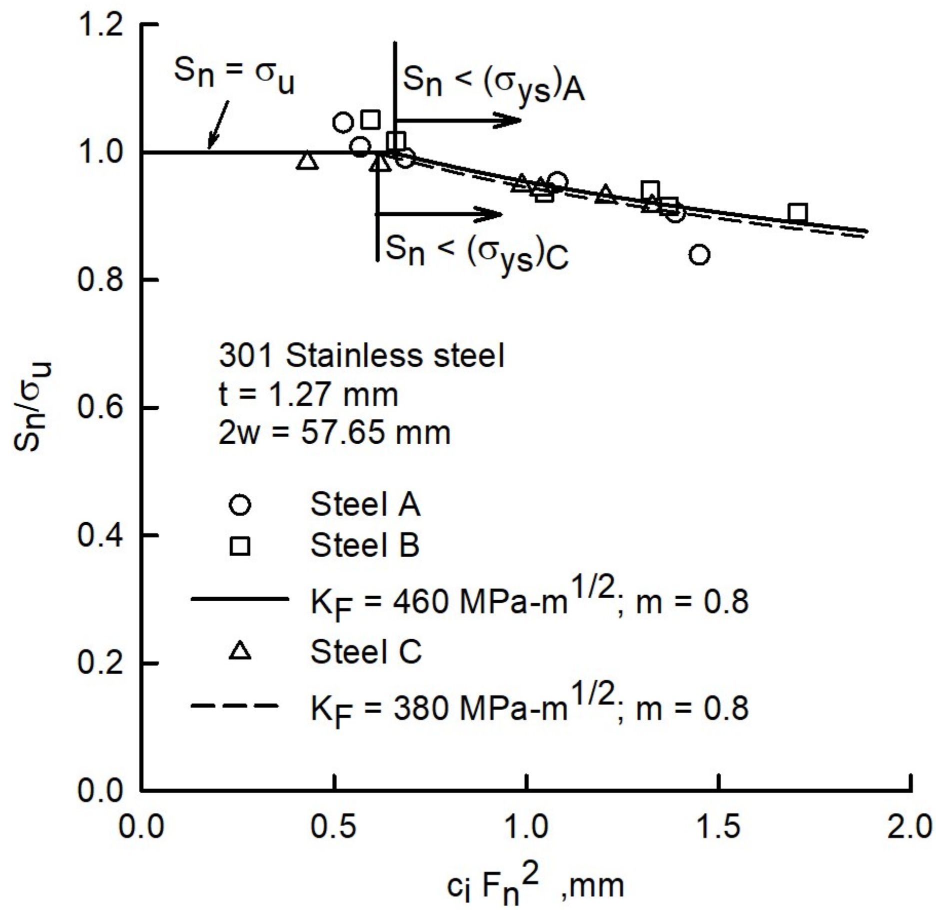

Figure 6.9 Net-section stress at failure normalized by ultimate strength against crack-tip parameter for Ardeformed 301 stainless steel.

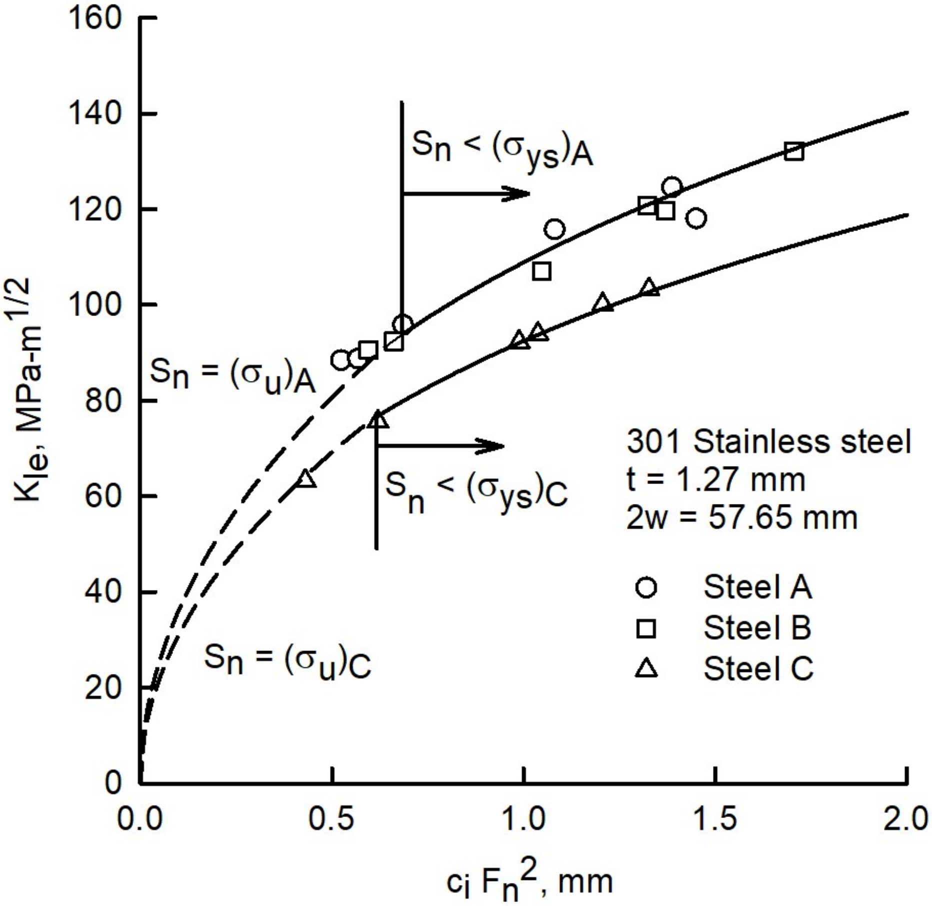

Figure 6.10 Critical stress-intensity factor at failure against crack-tip parameter for Aderformed 301 stainless steel.

CHAPTER VII

CONCLUDING REMARKS

The National Aeronautical and Space Administration (NASA) Marshall Space Flight Center (MSFC) has developed the Tool for Analysis of Surface Cracks (TASC) software. Allen and Wells, NASA MSFC, developed the TASC software. The software was used to calculate the critical parametric angle (ϕ_c) along a surface-crack front where fracture would initiate under remote tension. A surface crack in a sheet or plate of thickness, t, is defined by crack depth, a, and crack half-length, c. The determination of ϕ_c was based on maximizing the product of the J-integral and T-stress for different crack configurations (a/c, a/t) and material stress-strain properties using linear plus power-law hardening materials. The strain hardening coefficient was defined by n. Herein, strain hardening was considered from low strain hardening (n = 20) to very high strain hardening (n = 3). In the current study, a simple equation for the critical parametric angle was developed as a function of only crack shape (a/c) and crack size (a/t). The critical parameter angles were shown to be weakly dependent upon the strain-hardening coefficient.

After comparing the TASC software and the proposed equation for the critical parameter angles for fracture, an analysis was conducted on some of the crack shapes (a/c) and crack sizes (a/t) that had large differences between the two angles. The differences in the calculated stress-intensity factors at failure (K_{Ie}) were found to be insignificant, as the errors were less than 6.5%.

During this study, fracture test data on surface cracks in three materials: Ti-6Al-6V-2Sn, Ti-6Al-4V and 301 stainless steel were obtained from the literature. A fracture analysis was conducted on the three materials using the two-parameter fracture criterion (TPFC). From a least-squares procedure or averaging, the two fracture parameters, K_F and m, were found for each material. The TPFC correlated the fracture test data in three sheet materials very well, generally within about 5% of the experimental failure loads on the two ductile materials and within about 10% of the experimental failure loads for the brittle material.

The current research focused on conducting fracture analyses with the TPFC using the critical parameter angle equation for surface cracks under remote tension for crack-depth-to-crack-half-length ratios equal to or less than one ($a/c \leq 1$). Future studies should be conducted on surface cracks with $a/c > 1$ for tension and bending loads.

REFERENCES

[1] Irwin, G.R, "The crack extension force for a part through crack in a plate," Trans. ASME, J. appl. Mechs, Vol. 84, 1962, pp. 651-654.

[2] Green, A.E. and Sneddon, I.N., "The distribution of stress in the neighborhood of a flat elliptical crack in an elastic solid," Proc. Cambridge Phil. Soc, Vol. 46, 1950, pp. 159-164.

[3] Smith, F.W. and Alavi, M.J., "Stress intensity factors for a penny shaped crack in a half space," Engng. Fracture Mech., Vol. 3, 1971, pp. 241-254.

[4] Kobayashi, A.S. and Moss, W.L., "Stress intensity magnification factors for surface-flawed tension plate and notched round tension bar," Second International Conf. on Fracture, Brighton, England, 1969.

[5] Rice, J.R. and Levy, N., "The part-through surface crack in an elastic plate," Tech. Rept. NASA NCL 40-002-080/3, Div. of Engr., Brown Univ., Trans. ASME, J. Appl. Mech. Paper No. 71-APM-20, 1970.

[6] Smith, F.W., "Stresses near a semi-circular edge crack," University of Washington, Ph.D. Dissertation, 1966.

[7] Newman, J.C, Jr., "Fracture analysis of surface- and through-cracked sheets and plates," Engng. Fracture Mech., Vol. 5, 1973, pp. 667-689.

[8] Newman, J.C., Jr., and Raju, I.S., "Analyses of surface cracks in Finite Plates Under Tension or Bending Loads," NASA Technical Paper 1578, December 1979.

[9] Raju, I. S. and Newman, J. C., Jr., "Stress-intensity factors for a wide range of semi-elliptical surface cracks in finite-thickness plates," Engng. Fracture Mech., Vol. 11, No. 4, 1979, pp. 817-829.

[10] Kuhn, P., "Residual tensile strength in the presence of through cracks or surface cracks," NASA TN D-5432, National Aeronautics and Space Administration, Washington, D.C., 1970.

[11] Reuter, W.G., Newman, J.C., Jr., Macdonald, B.D. and Powell, S.R., "Fracture criteria for surface cracks in brittle materials," ASTM STP-1207, J. D. Landes, et al., Eds., 1994, pp. 617-635.

[12] Leach, A.M.; Daniewicz, S.R.; and Newman, Jr., J.C., "A new constraint based fracture criterion for surface cracks," Engng. Fracture Mech., Vol. 74, No. 8, 2007, pp. 1233–1242.

[13] ASTM E2899-15, "Standard test method for measurement of initiation toughness in surface cracks under tension and bending," ASTM International, West Conshohocken, PA., 2015.

[14] Allen, P.A. and Wells, D.N., "Elastic-plastic J-integral solutions for surface cracks in tension using an interpolation mMethodology," National Aeronautics and Space Administration Marshall Space Flight Center, NASA TM-217480, 2013.)

[15] Allen, P.A. and Wells, D.N., "Interpolation methodology for elastic-plastic J-integral solutions for surface cracked plates in tension," Engng. Fracture Mech, Vol. 119, 2014, pp 173-201.

[16] Smith, A.B., "Missile motor cases," American Society of Metals, Metals Engng. Quarterly, November 1963.

[17] Irwin, G.R., "Analysis of stresses and strains near the end of a crack traversing a plate," J. Appl. Mech., Vol. 24, 1957, pp. 361-364.

[18] Gross, B. and Srawley, J.E., "Stress-intensity factors for single edge notch specimens in bending or combined bending and tension by boundary collocation of a stress function," NASA TN D-2603, 1965.

[19] Newman, J. C., Jr., "A review and assessment of the stress-intensity factors for surface sracks," Part-Through Crack Fatigue Life Prediction, ASTM STP-687, 1979, pp. 16-42.

[20] Newman, J.C., Jr., and Raju, I.S., "Stress-intensity factor equations for cracks in three-dimensional finite bodies subjected to tension and bending loads," Computational Methods in the Mechanics of Fracture, Vol. 2, S. N. Atluri (ed.), 1986, pp. 311-334..

[21] Inglis, C.E., "Stresses in a plate due to the presence of cracks and sharp corners," Trans. Inst. Naval Architects, Vol. 55, 1913, pp. 219-241.

[22] Neuber, H., "Theory of stress concentration for shear-strained prismatical bodies with arbitrary nonlinear stress–strain law," J. Appl. Mech., Vol. 28, 1961, pp. 544–550.

[23] Newman, J.C., Jr., "Fracture analysis of various cracked configurations in sheet and plate materials," Properties Related to Fracture Toughness, ASTM STP-605, American Society for Testing and Materials, 1976, pp. 104-123.

[24] Newman, J.C., Jr., Reuter, W.G. and Aveline, C.R.: "Stress and fracture analyses of semi-elliptical surface cracks," ASTM STP-1360, 1999, pp. 403–423.

[25] Rice, J.R., "A path independent integral and the approximate analysis of strain concentration by notches and cracks," J. Appl. Mechs., Vol. 35, 1968, pp. 379-386.

[26] Wang, X., "Elastic T-stress solutions for semi-elliptical surface cracks in finite thickness plates," Engng. Fracture Mech., Vol.70, 2003, pp. 731-756.

[27] Wang, X. and Bell, R., "Elastic T-stress solutions for semi-elliptical surface cracks in finite thickness plates subject to non-uniform stress distributions," Engng. Fracture Mech., Vol. 71, 2004, pp. 1477-1496.